# A Study of Far Infrared IRAS Maps of Star Forming Region NGC 3603

**A Dissertation**

submitted to the
Central Department of Physics, Tribhuvan University, Kirtipur
in the Partial Fulfillment for the Requirement of
Master's Degree of Science in Physics

By

**Sudeep Neupane**
**June 1, 2012**

# Contents

# Recommendation

It is certified that **Mr. Sudeep Neupane** has carried out his masters dissertation work entitled **"A Study of Far Infrared IRAS Maps of Star Forming Region NGC 3603"** under my supervision.

He has carried out work on far infrared IRAS maps and studied the temperature and mass profile of the region of interest. He has also studied the inclination angle of the clouds.

I recommend the dissertation in the partial fulfillment for the requirement of Master's Degree of Physics.

............................................
Dr. Binil Aryal
Central Department of Physics
Tribhuban University, Kirtipur
Kathmandu, Nepal

Date: .............................

# ACKNOWLEDGEMENTS

I am grateful to a bunch of respected people without whom I would not be able to finish this dissertation successfully. Firstly I would like to thank my supervisor Associate Professor Dr Binil Aryal for providing an opportunity to work with him and for his guidance in each and every tiny steps working on the problems. Without his inspiring support, this dissertation would not come up in this form.

I am also thankful to our department head Prof Dr Lok Narayan Jha for his support and encouragement. I can not forget my professors Dr. Uday Raj Khanal, Dr. Mukunda Mani Aryal and all our faculties for being supportive all the time during my university days.

I am pleased to Dr Rishi Shah, Academician and a leading amateur astronomer of Nepal (NAST/NASO), who has always boosted me for pursuing a career in astrophysics and provided an opportunity working with him through Nepal Astronomical Society (NASO) in the field of astronomy education and outreach in Nepal. Completion of this work without the help of my colleagues from NASO would be much difficult.

I can not mention all the names here but I am indebt for the kind support of my friends Mr Riwaj Pokhrel, Mr. Toya Nath Chettri, Mr. Sudeep Jung Guring, Mr. Amrit Kafle, Mr. Tek Raj Adhikari, Mr. Dilli Ram Dhakal, and all the members of Astrophycis Research Group.

My deepest gratitude goes to my father Binod Prasad Neupane, my mother Saraswati Neupane and my brother Sudershan Neupane for being always there for me in any circumstances. Their understanding and support have played a great role to make me able to finish my masters' thesis and who I am today.

.

We certify that we have read this dissertation and in our opinion it is good in the scope and quality as dissertation in partial fulfillment for the requirement of Masters's Degree of Science in Physics.

## Evaluation Committee

Dr. Binil Aryal
(Supervisor)

Prof. Dr. Lok Narayan Jha
(Head)
Central Department of Physics
Tribhuban University, Kirtipur
Kathmandu, Nepal

External Examiner

Internal Examiner

Date:..........................

## ABBREVIATIONS

**A&A:** Astronomy and Astrophysics Journal
**AJ:** Astronomical Journal
**ApJ:** Astrophysical Journal
**ApJS:** Astrophysical Journal Suppliment
**Ap&SS:** Astrophysics and Space Science
**DEC:** Declination
**IRAS:** Infrared Astronomical Society
**MNRAS:** Monthly Notice of Royal Astronomical Society
**NED:** NASA Extragalactic Database (http://nedwww.ipac.caltech.edu/)
**PASJ:** Publications of the Astronomical Society of Japan
**pc:** Parsec ($=3.084\times10^{16}$)
**QJRAS:** Quarterly Journal of the Royal Astronomical Society
**RA:** Right Accession

**ABSTRACT**

**We studied the dust structure around two clumps of the star forming region NGC3603. For this, 100 $\mu$m and 60 $\mu$m IRAS maps of NGC3603 is downloaded from SkyView Virtual Observatory and processed in the software ALADIN2.5. We used the flux density emitted from the region of interest in order to calculate dust color temperature and dust mass of the region. In addition, a study of flux density variation along major and minor diameters of the clumps are conducted. Using Holmberg's formula, we estimated the inclination angle of the structure. Finally, a study of discrete source in the field of two clumps are carried out. In the large clump, the maximum and minimum values of the dust color temperature are 40.98 K and 27.39 K respectively. Total mass of the gas in the large clump is found to be $1.20\times10^4 M_\odot$. The small clump is found to be massive than that of the large clump. The dust color temperature is found to be lie in the range 24.80 - 39.61 K in the smaller clump. The total mass of the region of interest is about $3.10\times10^4 M_\odot$, greater than that of critical mass for 90.41 pc sized cloud. Thus, Jeans mass is found to be more than that of the critical mass, suggesting active star forming region. The flux density variation along major and minor diameter showed a Gussian like distribution, suggesting an isolated structure. The structure is found to be neither face-on nor edge-on type. A large number of stars are found to be surrounded near maxima of 100 $\mu$m emission of both large and small clumps, indicating on going star formation.**

# Chapter 1

# Introduction

## 1.1 Introduction

Although most of the mass in molecular cloud is in the form of molecular hydrogen, $H_2$ is largely invisible under quiescent interstellar conditions. Instead, observations of emission and absorption from dust and rotational lines from molecular species such as CO and its isotopologues are typically used as proxies to determine the properties of molecular clouds. Recent studies have shown that dense cores, the immediate precursors of stars, exist preferentially in the small percentage of molecular clouds with high column density, and that cores are strongly clustered (Enoch et al. 2006; Johnstone et al. 2004). In order to understand why dense cores form in certain regions and not others, how long cores can survive without either collapsing or dispersing, and a host of other star formation related issues, astronomers need to be able to determine such basic properties of molecular clouds as the temperature and mass profile of the dust and gas in the cloud.

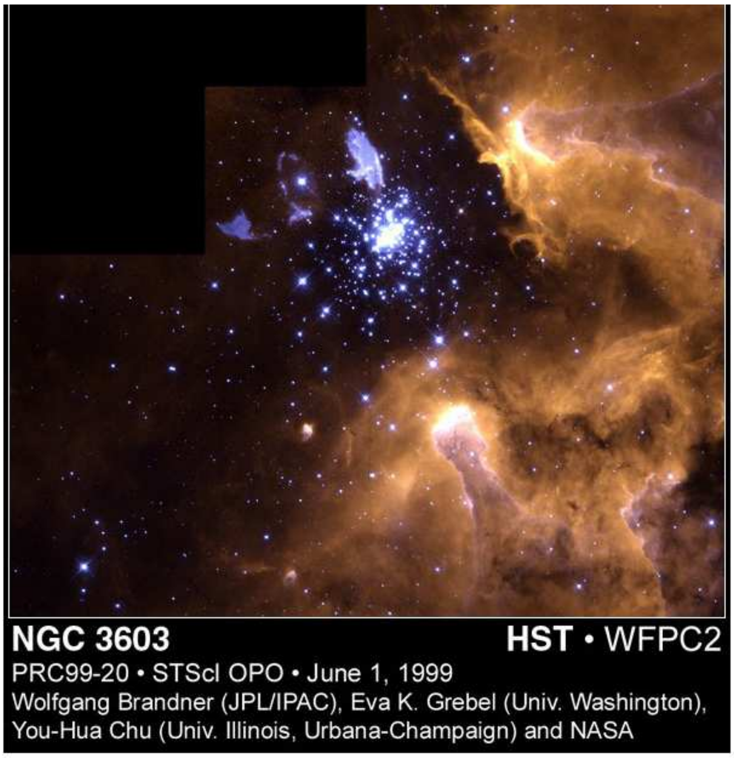


Figure 1.1: The optical image of NGC3603 obtained from Hubble Space Telescope. [Source: Web[1]]

The bulk of the molecular gas is contained in a molecular ring between 3.5 to 7.5 kpc from the center of the galaxy (the Sun is about 8.5 kpc from the center). Among them, NGC 3603 is an open cluster of stars situated in the Carina spiral arm of the Milky Way around 20,000 light-years away from the Solar System. This luminous very compact young star cluster is located at the center of the most massive visible HII region in our galaxy. Hubble Space

Telescope (HST) observations of the cluster region reveal a number of similarities with the core of R136 in 30 Doradus in the Large Magellanic Cloud (Moffat, Drissen and Shara 1994). NGC 3603 is considered a Galactic clone of the starburst cluster R136 in the LMC (Moffat, Drissen, and Shara 1994). The study of NGC 3603 could therefore be a first step toward an understanding of the nature and stellar content of a starburst cluster.

Surrounded by the most massive visible cloud of glowing gas and plasma known as a H II region in the Milky Way, NGC3603 emits strong ultraviolet radiation and also stellar winds have cleared the gas and dust, giving an unobscured view of the cluster. Due to the relatively low foreground extinction of $A_v \sim 4.5$ (Moffat 1983; Melnick et al. 1989), the NGC3603 OB cluster offers the unique opportunity to study its stellar content in great detail by optical photometry and spectroscopy.

Thus, to understand the properties of the NGC3603 molecular cloud and the effect from the surrounding sources, we planned to study the temperature and mass profile using IRAS 60 $\mu$m and 100 $\mu$m images.

## 1.2 Objectives

Our objectives to carry out this work is as follows:

1. We plan to study the distribution of dust color temperature and the mass of the gas in the region of interest to describe the physical property of the nebula. We will calculate and discuss the temperature and mass profile using suitable data reduction software.

2. We aimed to calculate the total mass of the region with the help of IRAS images.

3. We plan to study the flux density variation along the major and minor diameter of the clumps in the region of our interest.

4. Discrete point source in the field of the nebular region will be studied by using SIMBAD (http://simbad.u-strasbg.fr) database. Their interaction with the structure will be studied and discussed.

5. We intend to estimate inclination angle of the nebula in order to study its true structure.

# Chapter 2

# Theory

## 2.1 Interstellar Medium (ISM)

Although space is very empty and the stars in the Milky Way are very far apart, the space between the stars contains a very diffuse medium of gas and dust astronomers call the interstellar medium (ISM). This medium consists of neutral hydrogen gas (HI), molecular gas (mostly $H_2$), ionized gas (HII), and dust grains. It fills interstellar space and blends smoothly into the surrounding intergalactic space. The energy that occupies the same volume, in the form of electromagnetic radiation, is the interstellar radiation field. Although the interstellar medium is, by several orders of magnitude, a better vacuum than any physicists can create in the laboratory there is still about of 5-10 billion $M_\odot$ of gas and dust out there, comprising approximately 5 % of the mass of visible stars in the Galaxy (Smith H. E., 2012).

The interstellar medium is composed of multiple phases, distinguished by whether matter is ionic, atomic, or molecular, and the temperature and density of the matter. The thermal pressures of these phases are in rough equilibrium with one another. Magnetic fields and turbulent motions also provide pressure in the ISM, and are typically more important dynamically than the thermal pressure is.

In all phases, the interstellar medium is extremely dilute by terrestrial standards. In cool, dense regions of the ISM, matter is primarily in molecular form, and reaches number densities of $10^6$ molecules $cm^{-3}$(Dyson J., 1997). In hot, diffuse regions of the ISM, matter is primarily ionized, and the density may be as low as $10^{-4}$ ions $cm^{-3}$. Compare this with a number density of roughly $10^{22}$ $cm^{-3}$ for liquid water. By mass, 99 % of the ISM is gas in any form, and 1% is dust. Of the gas in the ISM, 89 % of atoms are hydrogen and 9% are helium, with 2% of atoms being elements heavier than hydrogen or helium, which are called "metals" in astronomical parlance. The hydrogen and helium are a result of primordial nucleosynthesis, while the heavier elements in the ISM are a result of enrichment in the process of stellar evolution.

The ISM of galaxies is the reservoir out of which stars are born and into which stars inject newly created elements as they age. The ISM is filled with tenuous hydrogen and helium gas and a sprinkling of heavier atoms. These elements can be neutral, ionized, or in molecular form and in the gas phase or in the solid state. This gas and dust is visibly present in a variety of distinct objects: HII regions, reflection nebulae, dark clouds, and supernova remnants.

The ISM plays a crucial role in astrophysics precisely because of its intermediate role between stellar and galactic scales. Stars form within the densest regions of the ISM, molecular clouds, and replenish the ISM with matter and energy through planetary nebulae, stellar winds, and supernovae. This interplay between stars and the ISM helps determine the rate at which a galaxy depletes its gaseous content, and therefore its lifespan of active star formation. ISM plays a central role in the evolution of the Galaxy. It is the repository of the ashes of previous generations of stars enriched by the nucleosynthetic products of the fiery cauldrons in the stellar interiors. These are injected either with a bang, in a supernova explosion, or with a whimper, in the much slower moving winds of low-mass stars on the asymptotic giant branch. In this way, the abundances of heavy elements in the ISM slowly increase. This is part of the cycle of life for the stars of the Galaxy, because the ISM itself is the birthplace of future generations of stars.

The physical properties of the interstellar medium are governed in part by the radiation emitted by these stars. Far-ultraviolet (6 eV$\leq$h$\leq$13.6 eV) photons from massive stars dominate the heating and influence the chemistry of the neutral atomic gas and much of the molecular gas in galaxies (Tielens, 2005). Predominantly neutral regions of the interstellar medium in which the heating and chemistry are regulated by far ultraviolet photons are termed Photo-Dissociation Regions (PDRs). These regions are the origin of most of the non-stellar infrared (IR) and the millimeter and submillimeter CO emission from galaxies. The importance of PDRs has become increasingly apparent with advances in IR and submillimeter astronomy.

## 2.2 Interstellar Dust

Interstellar dust is an important component of the interstellar medium. Dust provides the dominant opacity source in the interstellar medium for non-ionizing photons and therefore controls the spectral energy distribution of the ISM at all wavelengths longer than 912 $\mathring{A}$ (Tielens, 2005). It obscures all but the relatively nearby regions in visual and ultraviolet wavelengths, and reradiates the absorbed energy in the far-infrared part of the spectrum, thereby providing a major part ($\sim$ 30 %) of the total luminosity of the Galaxy.

Dust grains also lock up a substantial fraction of all heavy elements. Grains provide a surface on which species can accrete, meet, and react - giving rise to an interesting and complex chemistry. The physical processes involving dust, including their interaction with light - in particular their energy balance and the resulting temperature - and their charge balance are important to study dust properties. The composition of interstellar dust has been widely debated and silicates and graphite are generally considered the most important interstellar dust components. However, the discussion is very general and one might often substitute minerals for silicates and amorphous carbon for graphite in the discussion of the physical processes.

The FIR radiation from dust removes the gravitational energy of collapsing clouds, allowing star formation to occur. Dust also regulates the gas phase abundances of the elements through accretion and destruction processes.Dust is crucial for interstellar chemistry by reducing the ultraviolet (UV) radiation which causes molecular dissociations and providing the site of the formation of the most abundant interstellar molecule, $H_2$. Probably grain surfaces are responsible for other chemistry as well. Dust controls the temperature of the interstellar medium (ISM) by accounting for most of the elements which provide cooling, but also providing heating through electrons ejected photoelectrically from grains.

### 2.2.1 IRAS All Sky Survey

From 1983 January to November the Infrared Astronomical Satellite (IRAS), a joint project of the US, UK and the Netherlands (Neugebauer et al. 1984), performed a survey of 98 % of the sky at four wavelengths: 12, 25, 60 and 100 $\mu$m. IRAS let to numerous scientific discoveries spanning a board range of astrophysical subjects, from comets to circumstellar disks to interacting galaxies. The satellite was designed to optimized the reliability of point source detection and photometry; one of the great legacies of IRAS is certainly its catalog of more than 250,000 point sources. On the other hand, the relative stability of its detectors also allowed mapping of extended emission. In fact, IRAS made a significant contribution to our understanding of Galactic diffuse emission by revealing the interstellar dust emission of infrared cirrus, which can be observed in any direction on the sky.

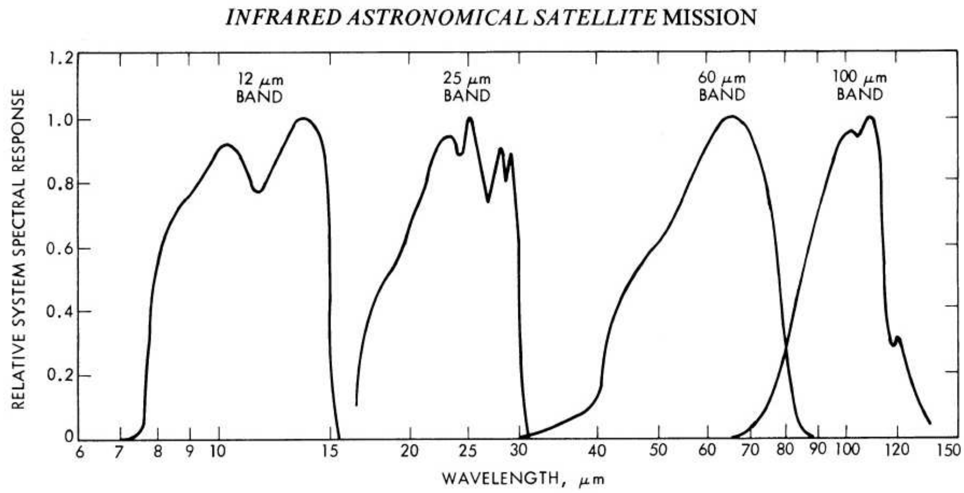


Figure 2.1: IRAS spectral response of the detector, field lens, and filter combinition of the survey array. Quoted, the flux densities have been calculated at wavelengths of 12, 25, 60, and 100 $\mu$m assuming the energy distribution of the source is flat in flux per logarithmic frequency interval. [Source: Neugebauer G. et al., 1984]

Unbiased and sensitive all sky survey at infrared wavelength are difficult because of the obscuration of the Earth's atmosphere and because of the thermal emission from warm telescopes and the atmosphere. The IRAS mission was designed to overcome these difficulties by conducting an all sky survey from space satellite with cooled telescope. The primary goal of IRAS was to survey more than 95 % of the sky at wavelengths from 10 to 100 $\mu$m with a sensitivity as close as practical to the limitation set by the fluctuations in the thermal emission from the zodiacal background.The original all sky survey has sensitivity limits for point sources of around 500 mJy at 12, 25, and 60 $\mu$m and 1.5 Jy at 100 $\mu$m (Beichman et al., 1985). The IRAS had a tremendous impact on many areas of modern astrophysics. In particular, it revealed the ubiquity of infrared cirrus that is a spectacular manifestation of the interstellar medium complexity but also an important foreground for observational cosmology. IRAS is a natural data set to study the variations of dust properties at all scales.

### 2.2.2 Dust Color Temperature Estimation

The fundamental idea for the calculation of dust color temperature from the IRAS 60 $\mu$m and 100 $\mu m$ flux densities is similar to Schnee et al. (2005). The temperature is determined by the ratio of the 60 $\mu$m and 100 $\mu$m flux densities. The dust temperature $T_d$ in each pixel of a FIR image can be obtained by assuming that the dust in a single beam is isothermal and that the observed ratio of 60 $\mu$m to 100 $\mu$m emission is due to black body radiation from dust grains at $T_d$, modified by a power law of spectral emissivity index. The flux density of emission at a wavelength $\lambda_i$ is given by

$$F_i = [\frac{2hc}{\lambda_i^3(e^{\frac{hc}{\lambda_i K T_d}} - 1)}] N_d \alpha \lambda_i^{-\beta} \Omega_i \tag{2.1}$$

where $N_d$ is the column density of dust grains, $\alpha$ is a constant which relates the flux with the optical depth of the dust, $\beta$ is the spectral emissivity index, and $\Omega_i$ is the solid angle subtended at $\lambda_i$ by the detector.

Following Dupac et al. (2003), we use the equation

$$\beta = \frac{1}{(\delta + wT_d)} \tag{2.2}$$

to describe the observed inverse relationship between temperature and emissivity spectral index.

With the assumptions that the dust emission is optically thin at 60 $\mu$m and 100 $\mu$m and that $\Omega_\omega \simeq \Omega_{100}$ (true for IRAS image), we can write the ratio, R, of the flux densities at 60 $\mu$m and 100 $\mu$m as

$$R = 0.6^{-(3+\beta)} \frac{e^{\frac{144}{T_d}} - 1}{e^{\frac{240}{T_d}} - 1} \tag{2.3}$$

The value of $\beta$ depends on dust grain properties like composition, size, and compactness. For reference, a pure blackbody would have $\beta = 0$, the amorphous layer-lattice matter has $\beta \sim 1$, and the metals and crystalline dielectrics have $\beta \sim 2$.

For a smaller value of $T_d$, 1 can be dropped from both numerator and denominator of Eq. (2.3) and it takes the form

$$R = 0.6^{-(3+\beta)} \frac{e^{\frac{144}{T_d}}}{e^{\frac{240}{T_d}}} \tag{2.4}$$

Taking natural logarithm on both sides of Eq. (2.4) we find the expression for the temperature as

$$T_d = \frac{-96}{ln\{R \times 0.6^{(3+\beta)}\}} \tag{2.5}$$

where R is given by

$$R = \frac{F(60\mu m)}{F(100\mu m)} \tag{2.6}$$

F(60 $\mu$m) and F(100 $\mu$m) are the flux densities in 60 $\mu$m and 100 $\mu$m respectively. One can use equation 2.5 for the determination of the dust grain temperature.

### 2.2.3 Dust Mass Estimation

The far infrared emission which is used for the derivation of the dust mass is measured from the 100 $\mu$m IRAS images, as the longer wavelength measurements give us more precise dust masses due to the characteristics of the Planck curve. Processed IRAS images of moderate resolution are retrieved from the IRAS server in Groningen (Assendorp et al. 1995), and flux measurements were carried out using the ALADIN2.5 software.

The dust masses are estimated from the infrared flux densities at 60 $\mu$m and 100 $\mu$m, following the calculation of Meaburn et al. 2000; Young et al. 1993, Donofrio et al. 1999 & Hildebrand 1983. The infrared flux can be measured from IRAS Sky-View images and images from the Groningen using ALADIN2.5 software. The background correction is done by subtracting the average flux emitted by the external sources other than the object of interest. The black body intensity can be calculated using the basic expression as given in equation (2.19). The resulting dust mass depends on the physical and chemical properties of the dust grains, the adopted dust temperature $T$ and the distance $D$ to the object.

$$M_{dust} = \frac{4}{3}\frac{a\rho}{Q_\nu}[\frac{S_\nu D^2}{B(\nu,T)}] \tag{2.7}$$

where,
$a$ = weighted grain size
$\rho$ = grain density
$Q_\nu$ = grain emissivity
$S_\nu$ = total flux density of the region whose mass is to be determined

The Planck's function is a well known function, given by this equation,

$$B(\nu,T) = \frac{2h\nu^3}{c^2}[\frac{1}{exp(\frac{h\nu}{KT})-1}] \tag{2.8}$$

where,
$h$ = Planck's constant
$c$ = velocity of light
$\nu$ = frequency at which the emission is observed
$T$ = the average temperature of the region (calculated using expression 2.5)

## 2.3 Infrared Astronomy

The branch of astronomy and astrophysics dealing with the objects visible in the Infrared Radiation (IR) is the infrared astronomy. The range of wavelength between 400 nm (blue) to 700 nm (red) is called the visible wavelength band. Longer wavelengths than 700 nm but shorter than microwaves are called infrared (or sometimes sub millimeter waves). Astronomers classified infrared astronomy as a part of optical astronomy because optical components (mirrors, lenses and solid state detectors) are usually used in investigating celestial objects. The infrared band is usually subdivided into the sub-millimeter, the far-(1 mm to 50 $\mu$m, FIR), mid-(50 $\mu$m to 10 $\mu$m, MIR) and near-infrared (10 $\mu$m to 1 $\mu$m, NIR) (Tielens 2005).

In the far infrared, stars are not generally bright, but we can observe the emission from very cold matter (140 K or less) which is not seen at smaller wavelengths (Simkhada 2006). Huge, cold clouds of dust and gas in our own galaxy, as well as in our nearby galaxies, glow in far infrared light. New stars are just beginning to form in some of these clouds. Far infrared observations can detect these protostars long before they turn on visibly by sensing the heat they radiate as they contract. The center of our galaxy also shines brightly in the far infrared because of the thick concentrations of the stars embedded in dense clouds of dust. These stars heat up the dust and cause it to glow brightly in the infrared.

Except for the plane of our galaxy, the brightest far infrared object in the sky is central region of galaxy called Meissner object (M82). The nucleus of M82 radiates as much energy in the far infrared as all of the stars in our galaxy combines. The origination of the far infrared energy is due to the heating of dust by a source which is hidden from view (Karttunen et al. 2007). The central regions of most galaxies shine very brightly in the far infrared. Most of the galaxies have active nuclei hidden in the dense regions of dust. These are known as active galaxies. The rest, called star burst galaxies, have an extremely high number of newly formed stars heating interstellar dust clouds. These galaxies, are the brightest among all galaxies in the far infrared.

Infrared radiation with wavelength close to that of visible light behaves similar to the visible light, and can be detected by using similar electronic devices. Due to this reason, the near infrared region is analyzed as a part of optical spectrum, along with near ultraviolet. The development of the infrared astronomy has revealed important information regarding the structures of various stellar phenomenon, star forming regions, discoveries of new celestial objects etc. When the objects emitting radiation move away from us, light emitted by them gets longer in wavelength and therefore they are said to be shifted to the red part of the optical spectrum. If these objects are moving towards us, the light emitted by them gets shorter in wavelength and they are said to be shifted to the blue part of the optical spectrum. The overall effect is known as Doppler effect i.e., red shift and blue shift respectively. The recession of galaxies away from us (red shift), which was confirmed by Edwin Hubble shows interesting effects in the light emitted from these galaxies (Palen 2002). As a result of the red shift almost all ultraviolet and most of the radiation in the visible region from distant sources (galaxies) is shifted to the infrared region of the spectrum and it reaches to our telescope when we observe. The only possible way to investigate this red shifted radiation is in the infrared region of the spectrum.

Using the analysis of the data compiled in the infrared activities of the celestial objects, astronomers have gathered various supporting facts about the evolution and the development of the universe which was believed to have begun with tremendous expansion known as Big Bang. In addition to this, the infrared investigation of the sky has revealed important information regarding galaxies, birth and death of stars, and particularly the dust grain properties of the interstellar medium.

Infrared observatories have been built on high mountain tops, where most of the atmospheric water vapour remains low. Some favorable sites are, e.g. Mauna Kea on Hawaii, Mount Lemon in Arizona and Pico del Teide on Tenerife. For observations in the far-infrared these mountains are not high enough; these observations are carried out, e.g. on aeroplanes. One of the best equipped planes is the Kuiper Airborne Observatory, named after the well-known planetary scientist Gerard Kuiper. Balloons and satellites are also used for infrared observations. The most successful infrared observatories so far have been the Infrared Astronomy Satellite IRAS and the European Infrared Space Observatory EISO. A very successful satellite was the COBE (Cosmic Background Explorer), launched in 1989, which mapped the background radiation in submillimeter and infrared wavelengths (Karttunen et al. 2007). Presently working infrared telescopes in the space are the Spitzer Space Telescope, the Wide-field Infrared Survey Explorer, Herschel Space Observatory and the Stratospheric Observatory for Infrared Astronomy SOFIA.

## 2.4 Molecular Cloud

A molecular cloud, sometimes called a stellar nursery if star formation is occurring within, is a type of interstellar cloud whose density and size permits the formation of molecules, most commonly molecular hydrogen ($H_2$). Molecular hydrogen is difficult to detect by infrared and radio observations, so the molecule most often used to determine the presence of $H_2$ is CO (carbon monoxide). The ratio between CO luminosity and $H_2$ mass is thought to be constant, although there are reasons to doubt this assumption in observations of some other galaxies. Within our own galaxy, molecular gas accounts for less than one percent of the volume of the interstellar medium (ISM), yet it is also the densest part of the medium comprising roughly one-half of the total gas mass interior to the Sun's galactic orbit. The bulk of the molecular gas is contained in a molecular ring between 3.5 to 7.5 kpc from the center of the galaxy (the Sun is about 8.5 kpc from the center)(Herter T., 2012). Large scale carbon monoxide maps of the galaxy show that the position of this gas correlates with the spiral arms of the galaxy. That molecular gas occurs predominantly in the spiral arms argues that molecular clouds must form and dissociate on a timescale shorter than 10 million years-the time it takes for material to pass through the arm region. Vertically, the molecular gas inhabits the narrow midplane of the Galactic disc with a characteristic scale height, Z, of approximately 50-75 parsec, much thinner than the warm atomic (Z=130-400 pc) and warm ionized (Z=1000 pc) gaseous components of the ISM (Basu S.K., 2007). The exception to the ionized gas distribution are HII regions which are bubbles of hot ionized gas created in molecular clouds by the intense radiation given off by young massive stars and as such they have approximately the same vertical distribution as the molecular gas. This smooth distribution of molecular gas is averaged out over large distances; however, the small scale distribution of the gas is highly irregular with most of it concentrated in discrete clouds and cloud complexes.

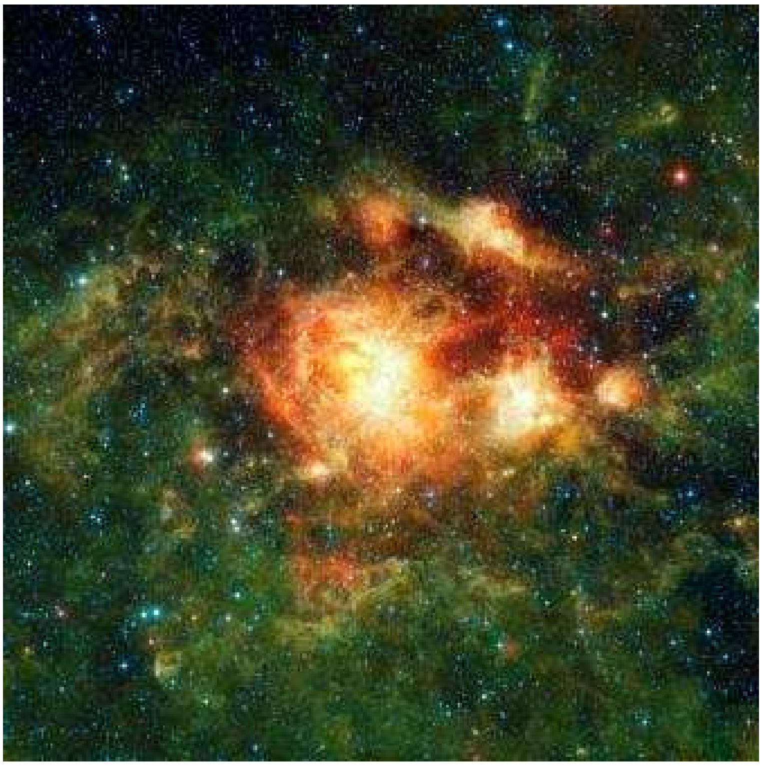

Figure 2.2: NGC3603 molecular cloud. This picture is one of the early release images of WISE. [Source: Web[2]]

The physics of molecular clouds are poorly understood and much debated. Their internal motions are governed by turbulence in a cold, magnetized gas, for which the turbulent motions are highly supersonic but comparable to the speeds of magnetic disturbances. This state is thought to lose energy rapidly, requiring either an overall collapse or a steady reinjection of energy. At the same time, the clouds are known to be disrupted by some process-most likely the effects of massive stars-before a significant fraction of their mass has become stars.

### 2.4.1 NGC 3603

NGC 3603 is an open cluster of stars situated in the Carina spiral arm of the Milky Way around 20,000 light-years away from the Solar System. NGC 3603 has been subject to intense study as a starburst region for more than a century because it represents a unique combination of proximity, low visual extinction, brightness and compactness.

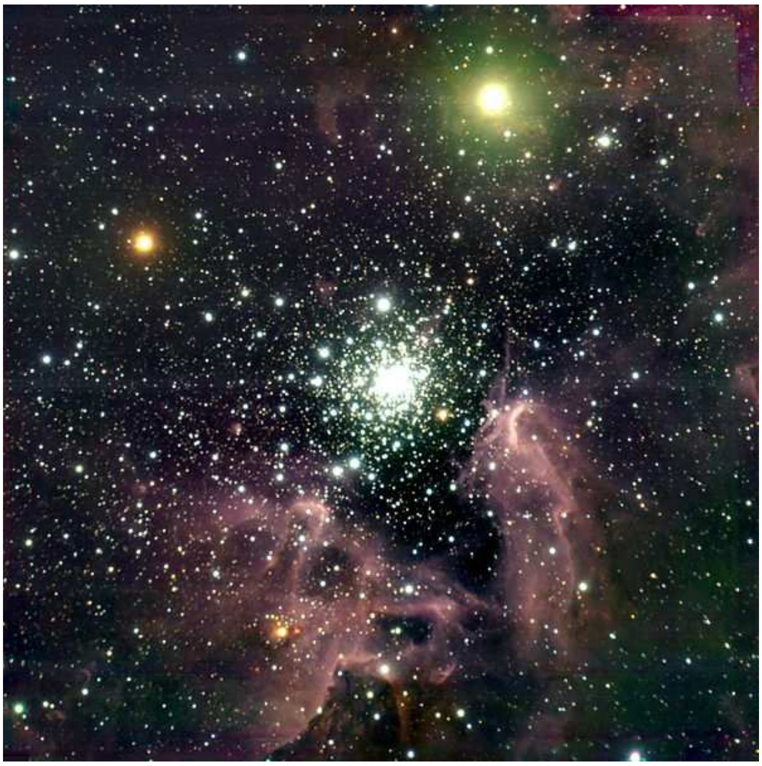

Figure 2.3: OB cluster in NGC3603. Image of the NGC 3603 region were obtained in three near-IR filter bands (Js, H and Ks) with the ISAAC instrument at the ANTU telescope. [Source : Web[3]]

This is a luminous, very compact young star cluster which is located at the center of the most massive visible HII region in the Carina arm. Its core contains a Trapezium-like system (HD 97950) with about 50 massive stars within a radius of a few arc seconds (Moffat 1983). Hubble Space Telescope (HST) observations of the cluster region reveal a number of similarities with the core of R136 in 30 Doradus in the Large Magellanic Cloud (Moffat, Drissen and Shara 1994).

It was observed by John Herschel on the 14th of March 1834 during his visit to South Africa, who remarked that it was “a very remarkable object perhaps a globular cluster”. Herschel catalogued it as nebula 3334 in his Results of Astronomical Observations made at the Cape of Good Hope, published in 1847. In 1864 the Royal Society published his General Catalogue of Nebulae and Clusters, where he listed it as number 2354. It was subsequently incorporated into the New General Catalogue as by J. L. E. Dreyer as NGC 3603.

It is surrounded by the most massive visible cloud of glowing gas and plasma known as a H II region in the Milky Way. HD 97950 is the central star of star cluster, the densest concentration of very massive stars known in the galaxy. Strong ultraviolet radiation and stellar winds have cleared the gas and dust, giving an unobscured view of the cluster.

Three prominent Wolf-Rayet stars have been detected within the cluster. These three massive stars have been observed and their solar mass measured using the Very Large Telescope. The largest of the three, NGC 3603-A1 is a blue double star that orbit around each other once every 3.77 days. The two combined have a solar mass that is 200 times more massive than our Sun: (A1-a) is the largest known star in our galaxy with an estimated mass of 116 solar masses, while its companion (A1-b) has a mass of 89 solar masses.

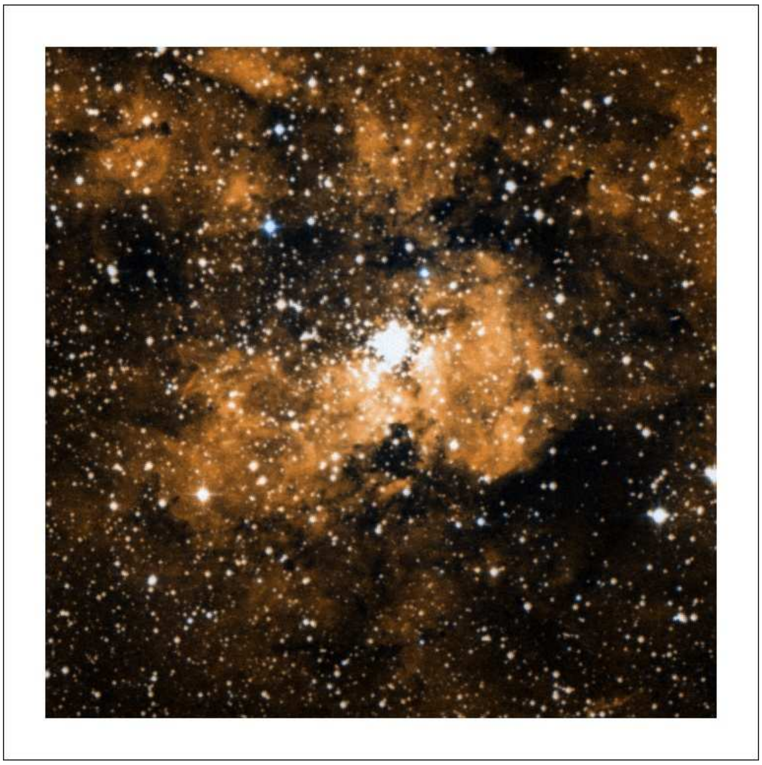

Figure 2.4: An optical view of NGC3603 showing the glowing gas and plasma around the star cluster.[Source: Web[4]]

NGC 3603 is visible in the telescope as a small rather insignificant nebulosity with a yellowish tinge due to the effects of interstellar absorption. In the mid-1960s optical studies coincided with radio astronomical observations which showed it to be an extremely strong thermal radio source. Later observations in other galaxies introduced the concept of "starburst" regions, in some cases whole galaxies, of extremely rapid star formation and NGC 3603 is now considered to be such a region.

### 2.4.2 Structure and Content of NGC3603

A CCD UBV photometric study by Melnick et al.(1989) found a mean value of E (B-V) = $1.44 \pm 0.13$ mag which is in agreement with the earlier estimate by Moffat (1974). They derived an average age of 2∼3 Myr and showed that star formation is an on-going process in NGC 3603. Based on CCD observations, Pandey, Ogura and Sekiguchi (2000) studied in detail the reddening of the cluster members and found an anomalous reddening law with radial variation in the intracluster material. The stellar content of NGC 3603 has been studied using speckle-masking observations (Hofmann, Seggewiss and Weigelt 1995) and adaptive optics nearinfrared imaging from the ground (Eisenhauer et al. 1998).

Its core contains many early O-type stars as well as three WN6 stars; NGC 3603 is considered a Galactic clone of the starburst cluster R136 in the LMC (Moffat et al., 1994). The study of NGC 3603 could therefore be a first step toward an understanding of the nature and stellar content of a starburst cluster. The cluster is so compact that it was previously considered a multiple star (van den Bos 1928). This has made it difficult to study the cluster in detail from classical groundbased telescopes. The construction of large ground-based telescopes, the introduction of new technologies−adaptive optics and active opticsand the availability of space telescopes now make it possible to study the cluster in unprecedented resolution both in the spatial and spectral domain.

Moffat (1983) studied the stellar content of NGC 3603. He presented spectral types of 13 stars in NGC 3603 and confirmed the WN nature of the central multiple system HD 97950 (Walborn 1973). He also found several low-luminosity early O-type stars, as well as three evolved O-, B-type supergiants, and as a result suggested noncoeval star formation in NGC 3603. Melnick et al. (1989) obtained UBV CCD photometry and determined the distance and age of the cluster. They also tried to measure the magnitudes of stars near the center, but their values were strongly affected by crowding.

The structure and kinematics of the interstellar medium around NGC 3603 was also investigated. Balick et al. (1980) studied the structure and kinematics using a pressure-scanned Fabry-Perot interferometer and found a small wind-driven stellar bubble. Clayton (1986) studied the gas motion of the giant H II region in detail. He found major splitting or asymmetry in Ha with peak-to-peak velocity differences of up to 150 km $s1$. He suspected that these large-scale motions were set up before the formation of NGC 3603, possibly by the action of earlier supernovae.

In the 1990s much progress was made in the study of the stellar content of NGC 3603 using data from HST and large ground-based telescopes. Moffat et al. (1994) used HST/PC1 images to study the stellar content in the core of NGC 3603 and compared it with R136 in 30 Dor. They found that for stars brighter than $M_v$ = -5.0, the central densities were very similar, but outside r $\approx$1 pc the density of massive stars in NGC 3603 plummets to zero, while in 30 Dor it continues to decrease out to r $\approx$ 130 pc. Drissen et al. (1995) obtained spectra of 14 individual luminous stars in NGC 3603 using HST/FOS. They resolved the central core of NGC 3603 and confirmed three WN6+abs stars and many early O-type stars. Hofmann et al. (1995) deconvolved the core region of NGC 3603 (HD 97950) from diffraction-limited speckle masking observations and obtained an age (3.2 Myr) and somewhat steep IMF ($\Gamma$ = -1.59) for the most massive stars (m =15 $M_\odot$).

Brandner et al. (1997) found a ring nebula and bipolar outflows associated with the B1.5 supergiant Sher 25. From the high-resolution echelle spectra, the northeast nebula shows an enhancement in nitrogen, this suggests that Sher 25 is an evolved postred supergiant. They also discussed the relation between Sher 25 and NGC 3603 and suggested that the starburst in NGC 3603 might have been triggered by the first generation of massive stars through their interaction with a dense cloud core (see also Drissen et al. 1995; Moffat 1983; Melnick et al. 1989). Brandner et al. (2000) discovered three protoplanetary disk (proplyd)-like objects in NGC 3603 whose spectral characteristics are very similar to those of an ultra-compact H II region with electron densities well in excess of $10^4$ cm-3. However, Nürnberger and Stanke (2003) could find no mid-infrared counterparts for the proplyd-like objects and concluded that they are smaller scale versions of the neighboring pillars.

Eisenhauer et al. (1998) studied for the first time the lowmass PMS stars in NGC 3603 using near-IR images from the adaptive optics system ADONIS on the 3.6 m telescope at La Silla. Their results suggest that low-mass PMS stars are forming even in a massive, starburst cluster. They also obtained the IMF down to subsolar-mass stars and derived a somewhat flat IMF $\Gamma$ = -0.7. Later, Brandl et al. (1999) confirmed the existence of low-mass PMS stars in NGC 3603 down to 0.1 $M_\odot$ from deep near-IR images obtained with the Very Large Telescope Antu unit. Using deep Ks-band images obtained with the infrared camera ISAAC on Antu, Nürnberger and Petr-Gotzens (2002) determined a radius ($r=150''\pm15''$) and studied the Ks-band luminosity function of the cluster. They also found that the slope of the IMF down to M $\sim$ 0.5 $M_\odot$ is consistent with that of a Miller-Scalotype IMF.

Frogel, Persson, and Aaronson (1977) studied several southern H II regions in the mid-IR. They found 15 mid-IR sources in NGC 3603, including the near-IR point source IRS 9. Later IRS 1 and 2 were found not to be point sources, but instead the head of a bright pillar (IRS 1) or an opaque protrusion (IRS 2) (Nürnberger and Stanke 2003). Recently, Nürnberger and Stanke (2003) studied NGC 3603 in the mid-IR using images obtained with TIMMI2 mounted on the ESO 3.6 m telescope. They found 36 mid-IR point sources, mid-IR emission from the three Wolf-Rayet stars WR 43abc, and a number of faint mid-IR sources with very red (K-N) colors. In addition, from the subarcsecond mid- IR image, they found two more point sources around IRS 9, the strongest mid-IR source in NGC 3603. Nürnberger(2003) studied the spectral energy distribution and near- and mid-IR colors of the embedded IR source IRS 9AC and suggested that they are a sparse association of high-mass protostars. The main source of ionization in NGC3603 is a massive cluster of OB and Wolf-Rayet stars (Goss and Radhakrishnan 1969), which shows - apart from the Galactic center region - the highest density of high mass stars known in the Galaxy (Melnick et al. 1989; Moffat et al. 1994; Drissen et al. 1995; Hofmann et al. 1995). Due to the relatively low foreground extinction of $A_v \sim 4.5$ (Moffat 1983; Melnick et al. 1989), the NGC3603 OB cluster offers the unique opportunity to study its stellar content in great detail by optical photometry and spectroscopy.

### 2.4.3 Distance Estimation

From photographic photometry, Sher (1965) obtained a distance of 3.5 kpc for NGC3603 OB cluster. However, Moffat (1974) derived a much larger distance of 8.1$\pm$0.8 kpc, in agreement with the kinematical distance of 7.2 $\pm$ 0.9 kpc (van den Bergh 1978). A distance of 5.3 $\pm$ 1.4 kpc to the cluster has been derived by Melnick and Grosbol (1982) using electronographic UBV photometry. On the other hand, Melnick and Grosbl (1982) determined a somewhat smaller value. Currently the accepted value is about 7 ± 1 kpc (Nürnberger and Stanke 2003).

### 2.4.4 HII Region

NGC3603 is the unique object; it is often described as most massive, optically visible giant H II region in the Galaxy (Goss, Radhakrishnan 1969). HII regions are regions of partially ionized hydrogen surrounding very hot young stars with spectral type O or B ($T_{eff} > 25000$ K), which emit copious amounts of photons beyond the Lyman limit ($h\nu > 13.6$ eV) and ionize and heat their surrounding, nascent molecular clouds. The gas in these regions is ionized and has a temperature of about $10^4$ K (Kundt 2005). Density range from $10^3$-$10^4$ $cm^{-3}$ for compact ($\sim 0.5$ pc) HII regions such as the Orion Nebula to $\sim 10$ $cm^{-3}$ for more diffuse and extended nebulae such as the North America Nebula ($\sim 10$ pc). The optical spectra of these regions are dominated by H and He recombination lines and collisionally excited, optical (forbidden) line emission from trace ions such as [OII], [OIII], and [NII]. HII regions are also strong sources of thermal radio emission from the ionized gas and of infrared emission due to warm dust. They are, therefore, signposts of sites of massive star formation in the Galaxy.

### 2.4.5 Photo Dissociation Region (PDR)

Observations have shown sharp PDR interfaces between the HII region and the molecular cloud in NGC3603. One important aspect of the study of PDR is to understand the process of star formation. The study of PDRs is the study of the effects of stellar far-utraviolet photons on the structure, chemistry, thermal balance, and evolution of the neutral interstellar medium of galaxies. Far-ultraviolet photons not only illuminate star- forming regions, causing them to glow in infrared emission, diagnostic of the physical conditions, but they may also play an important role in regulating the star formation process.

Historically, observational study of PDRs goes back to the early parts of 20th century, when optical absorption lines seen in the spectra of stars were shown to originate in interstellar rather than stellar photospheric gas. Much of this absorption occurred in relatively transparent neutral clouds called diffuse clouds, which often are identical to the cold neutral-medium phase (n$\sim$30 cm23 and T $\sim$100 K) of the ISM. Theoretical models of diffuse clouds appeared in the 1970s (e.g. Glassgold and Langer, 1974, 1976; Black and Dalgarno, 1976, 1977), stimulated by observations with the Copernicus space-borne telescope of ultraviolet absorption lines of trace quantities of rotationally excited H2 and other species (reviewed by Spitzer and Jenkins, 1975). Somewhat later, thicker molecular clouds ($A_v \sim 2$ 5), still studied through absorption lines in stellar spectra, were labeled translucent clouds.

The study of dense PDRs on the surfaces of opaque ($A_v \sim 2$) molecular clouds was stimulated by the observations of the massive star-forming regions Orion A and M17 in the fine-structure lines [CII] 158 mm and [OI] 63 mm by Melnick, Gull, and Harwit (1979), Storey, Watson, and Townes (1979)). The early [CI] 609 m observations of extensive columns of atomic carbon in molecular clouds also stimulated the modeling and understanding of dense

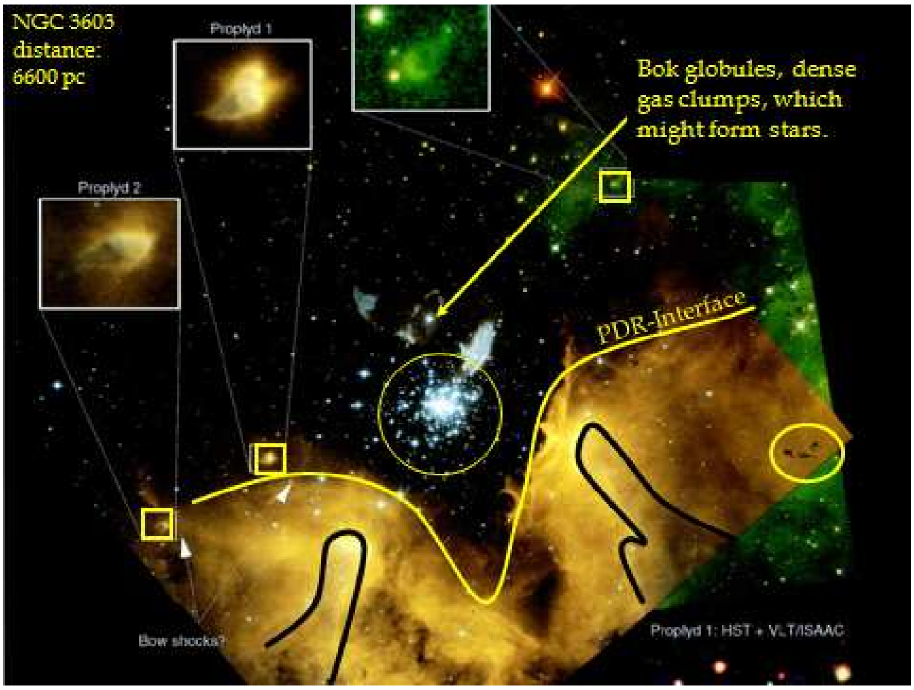


Figure 2.5: PDR interface in NGC3603.[Source: Web[5]]

PDRs (Phillips and Huggins, 1981; Keene et al., 1985). These observations pointed to predominantly neutral, infrared-luminous regions lying outside the HII regions.

Molecules in these PDRs are photodissociated and, for elements like carbon with ionization potentials below 13.6 eV, largely photoionized by the far-ultraviolet fluxes generated by nearby O star. The luminosity in the [CII] and [OI] lines, which dominate the cooling of the atomic gas, is of order $10^{-3}$ to $10^{-2}$ of the infrared (IR) luminosity from the dust that absorbed the starlight.

Despite these historical roots, the study of PDRs is not simply the study of diffuse and translucent clouds and the photodissociated gas that lies just outside of dense, luminous HII regions in the Galaxy; it includes as well the pervasive warm neutral medium, giant molecular clouds, reflection nebulae, the neutral gas around planetary nebulae, photodissociated winds from red giant and asymptotic giant branch stars, and the interstellar medium in the nuclei of starburst galaxies and galaxies with active galactic nuclei. PDRs include all interstellar regions where the gas is predominantly neutral but where far-ultraviolet photons play a significant role in the chemistry and/or the heating.

Traditionally, PDRs have been associated with atomic gas. However, PDRs include material in which the hydrogen is molecular and the carbon mostly in CO, but where far-ultraviolet flux still strongly affects the chemistry of oxygen and carbon not locked in CO (photodissociating OH, $O_2$, and $H_2O$, for example) and the ionization fraction. The transition from C1 to CO occurs in PDRs, and CO is arguably the most important molecule in astrophysics. Although $H_2$ is more abundant, CO is more readily observed and has been used extensively

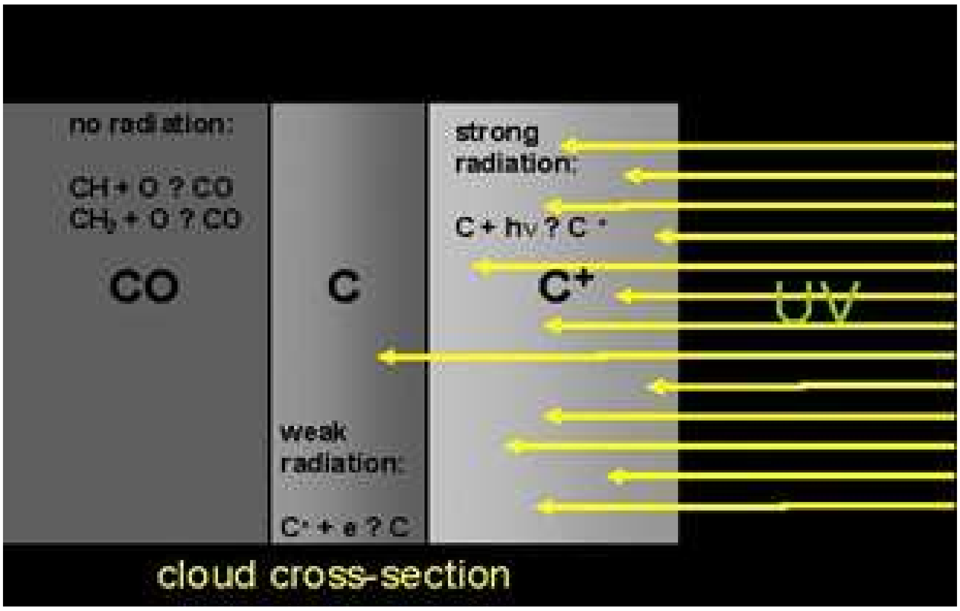


Figure 2.6: A schematic view of Photo Dissociation Region. The PDR is illuminated from right by strong FUV field. The PDR extends from the H+/H transition region through the H/H2 and C+/C/CO transitions until the O/O2 boundary. It thus includes the predominantly neutral atomic surface layer as well as large columns of molecular gas. [Source: Röllig 2010]

as a tracer of molecular gas and star-forming regions. With the exception of the molecular gas in dense, star-forming cores, most molecular gas in the Galaxy is found at $A_v$ less than or equal to 10 in giant molecular clouds. Therefore, the entire atomic and at least 90% of the molecular gas in the Galaxy is in PDRs.

### 2.4.6 Clumps of Molecular Gas in NGC3603

Nürnberger et al (2002) for the first time presented the large scale map of the dense molecular gas associated with NGC3603. Molecular cloud clumps which are detected in both CS(2-1) and CS (3-2) are lebeled MM1 through MM13.

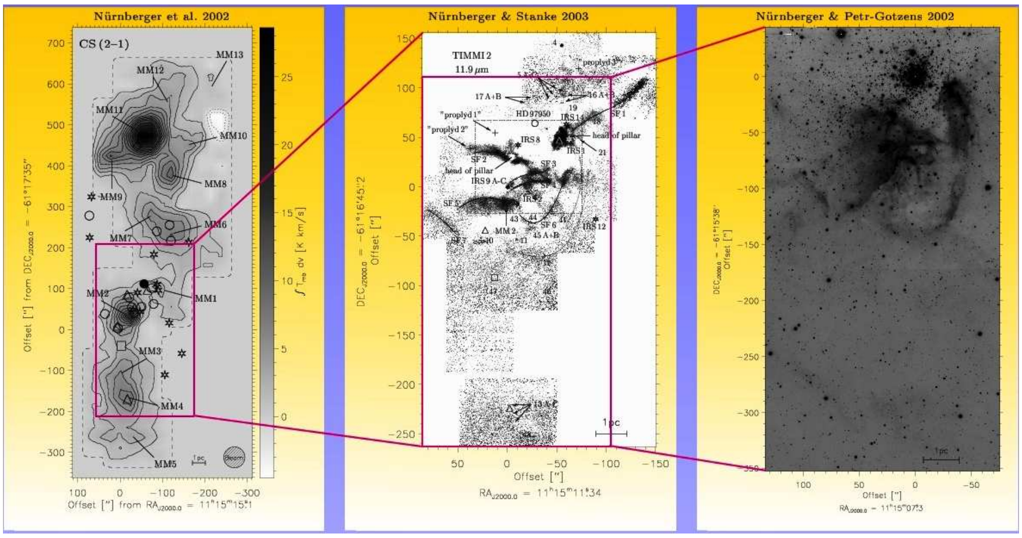


Figure 2.7: Molecular clumps in NGC3603 [Source: Nürnberger et al., 2002]

They proposed, on average, the molecular clumps have radii smaller than r $\sim$ 0.8 $\pm$ 0.2 pc, virial masses $M_{vir} \lesssim (1.0 \pm 0.6) \times 10^3 M_\odot$ and column densities $N(H_2) \gtrsim (0.4 \pm 0.2) \times 10^{23}$ cm$^{-2}$. Clump MM11 stands out with a 4 times higher mass and column density.

# Chapter 3

# The Region of Interest

## 3.1 Systematic Search in the IRAS Map

We carried a systematic search of IRAS maps available in the Skyview Virtual Observatory (http://skyview.gsfc.nasa.gov). SkyView is a Virtual Observatory on the internet generating images of any part of the sky at wavelengths in all regimes from Radio to Gamma-Ray.The skyView allows the users to search for the required image of the object with varying position, pixel size and different surveys.

We gave the required parameters for NGC3603 and the systematic search consists of the following steps.

Step-I:

**Inspection of the region in** $0.9° \times 0.9°$**,** $1° \times 1°$**,** $3° \times 3°$**,** $4° \times 4°$**,** $5° \times 5°$**, in Skyview Virtual observatory:**

The following input parameters were used for the search:

Coordinate: Equatorial
Projection: Rectangular
Image size (pixel): 300×300, 500×500
Brightness Scaling: Histogram Equilization
Name Resolver: SIMBAD/NED
Equinox: 2000 Color
Table: B−W Linear
Smoothing: 1
Image at Pixel Center: No
Pixel Resampling: Nearest Neighbor

Step-II:

**Download the FITS images of the selected region:**
We selected FITS format of the image to download for the data processing. The FITS image carries the information concerning the flux density, positions, etc. for each pixels.

Step-III:

**Analysis of the selected regions using ALADIN2.5 software:**
FITS image of the selected region were processed using software ALADIN2.5

## 3.2 Region of Interest: NGC3603

We looked for the star forming region in the northern sky and we found NGC3603 as an interesting object. NGC 3603 has been subject to intense study as a starburst region for more than a century because it represents a unique combination of proximity, low visual extinction, brightness and compactness. It is surrounded by the most massive visible cloud of glowing gas and plasma known as a H II region in the Milky Way. We planned to work on NGC3603 structure with the help of 60 and 100 $\mu$m IRAS images to study the temperature and mass profile along with the inclination angle of the molecular clumps.

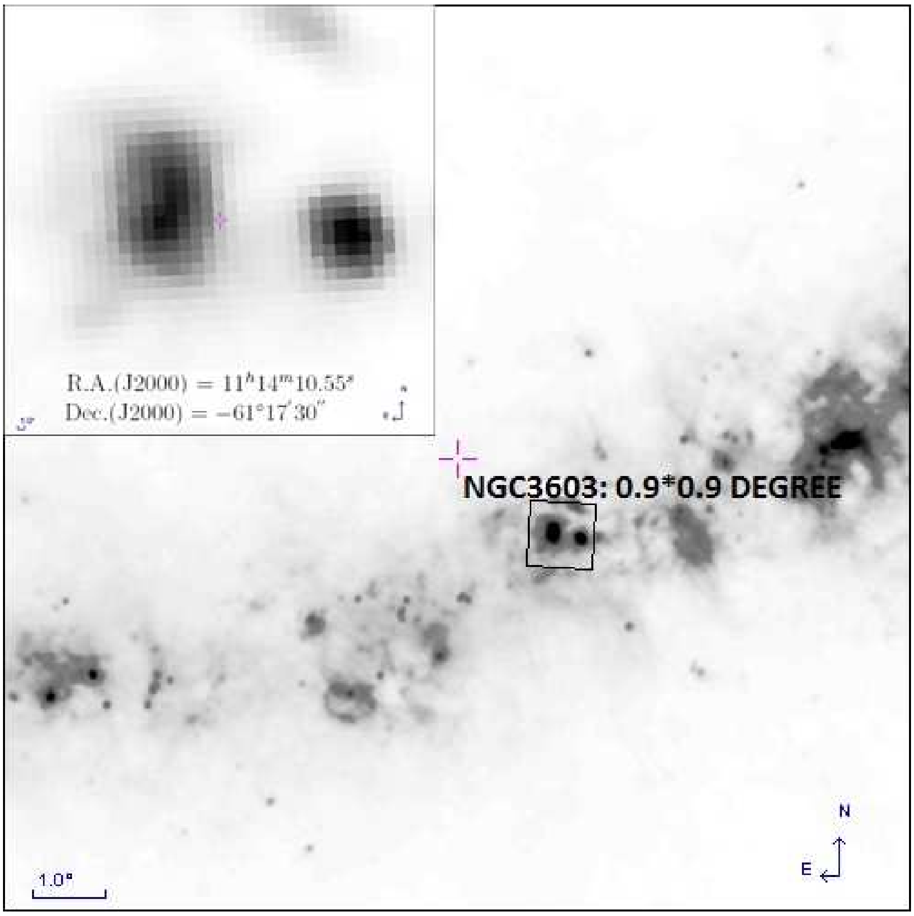


Figure 3.1: NGC3603 in a wide view (1024 x 1024 pixels)and our region of interest in zoomed view on the upper side.

We downloaded the FITS image of the NGC3603 centered at R.A.(J2000) = $11^h14^m10.55^s$ and Dec.(J2000) = $-61°17'30''$. These images, also shown below, are downloaded with pixel size 500×500 and degree size 0.9°×0.9°.

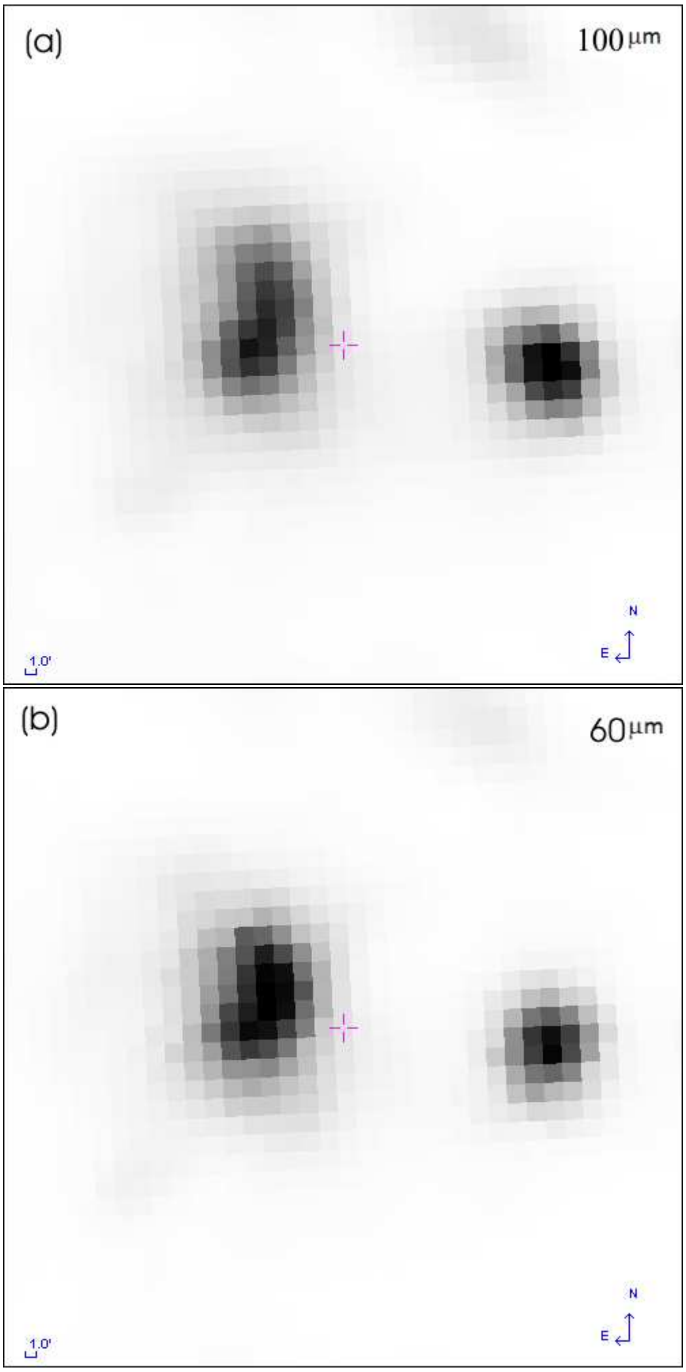


Figure 3.2: (a) $0.9^\circ \times 0.9^\circ$ IRAS 100 $\mu$m image, (b) $0.9^\circ \times 0.9^\circ$ IRAS 60 $\mu$m image. Both the images are centered at R.A.(J2000) $11^h14^m10.55^s$ and Dec.(J2000) $-61^\circ17'30''$.

# Chapter 4

# Methods of Analysis

## 4.1 Data Reduction

**ALADIN Software**
Aladin is an interactive software sky atlas allowing the user to visualize digitized astronomical images, superimpose entries from astronomical catalogues or databases, and interactively access related data and informatioin from the Simbad Database,SkyView, the VizieR service and other archives for all known sources in the field. Created in 1999, Aladin has become a widely used Virtual Observatory (VO) tool capable of addressing challenges such as locating data of interest, accessing and exploring distributed data sets, visualixzing multi-wavelength data. Compliance with existing or emerging VO standards, interconnection with other visualisation or analysis tools, ability to easily compare heterogeneous data are key topics allowing Aladin to be a powerful data exploration and integration tool as well as a science enabler. Aladin has been developed and is maintained by the Centre de Donnees astronomiques de starsbourg - France (CDS)(http://aladin.u-strasbg.fr/).

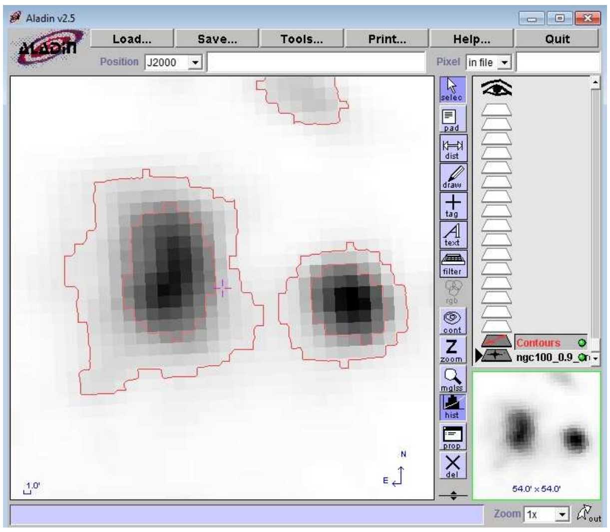


Figure 4.1: Schematic view of Software ALADIN2.5. [Source: Web[6]]

We have extensively used Aladin software (ALADIN2.5)to generate data from IRAS images downloaded from SkyView in 60 micron and 100 micron. We obtained the coordinates and relative flux densities of each pixel of the region of our interest using this software. Aladin also allowed us to draw contour lines and to obtain the distances for investigating different properties of our region of interest.

## 4.2 Contour Map

To investigate our region of interest, we used the method of drawing contours at different levels. Firstly, we examined in which contour level the regions have fair separation.

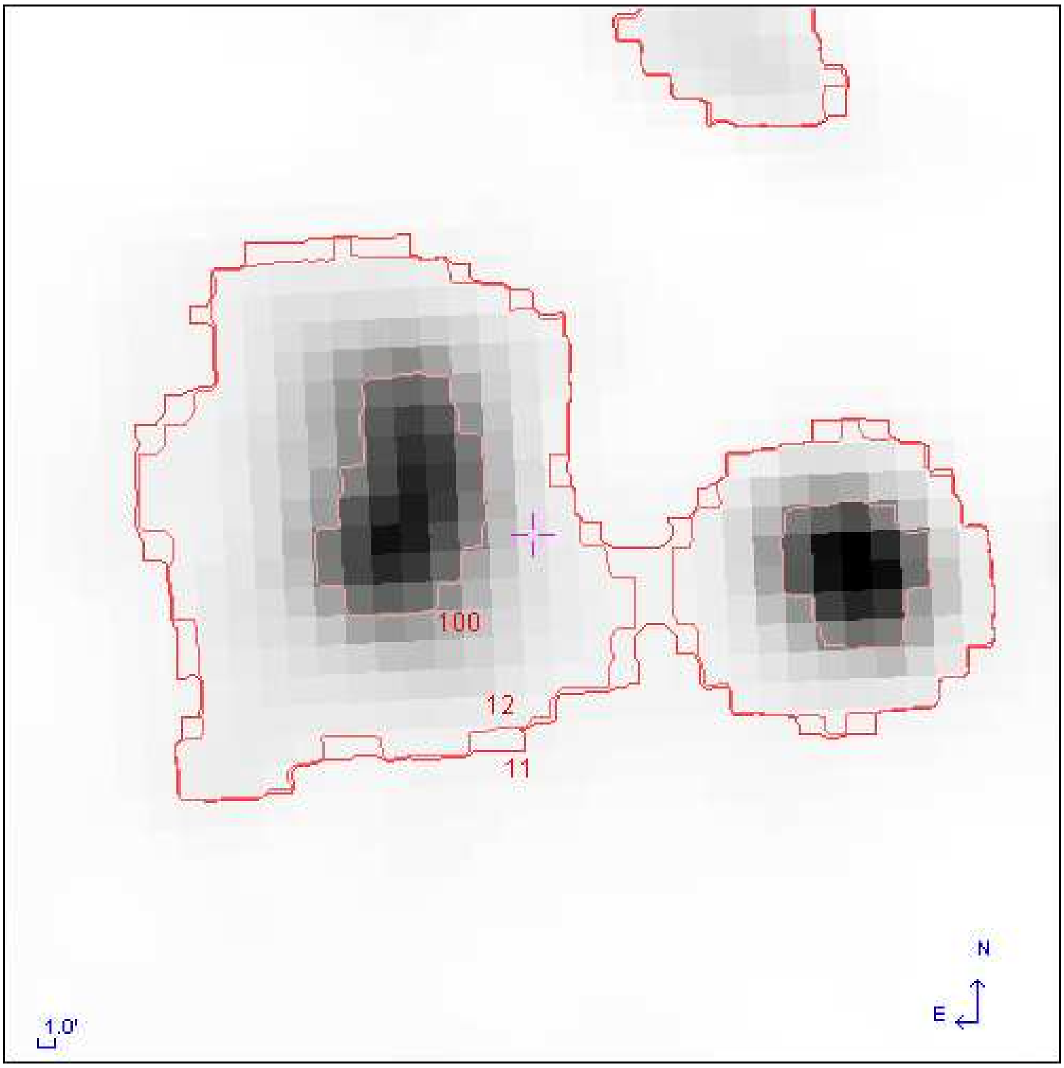


Figure 4.2: Contours at level 11, 12 and 100 drawn in 100 $\mu$m IRAS image. We also used the same contours to calculate the temperature and mass profile of the enclosed areas covered by the contours.

We planned to study the temperature and mass profile of the maxima regions in different clumps of the molecular cloud. We then separated the cloud choosing a desired contour by hit and trial method and found that the separation of the clumps at contour level 12 of IRAS 100 $\mu$m image.

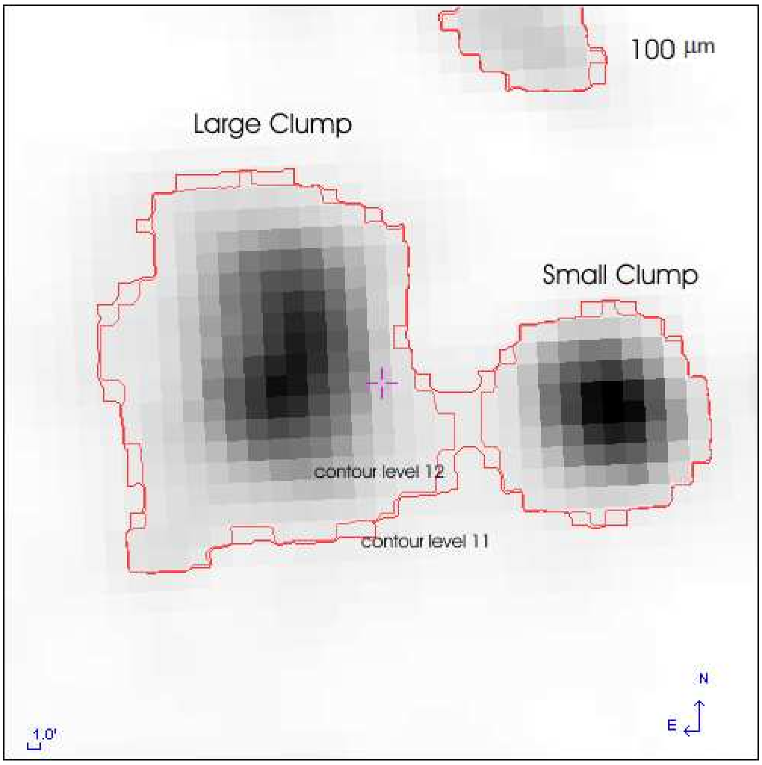


Figure 4.3: Clump separation at contour level 12 in 100 micron IRAS image.

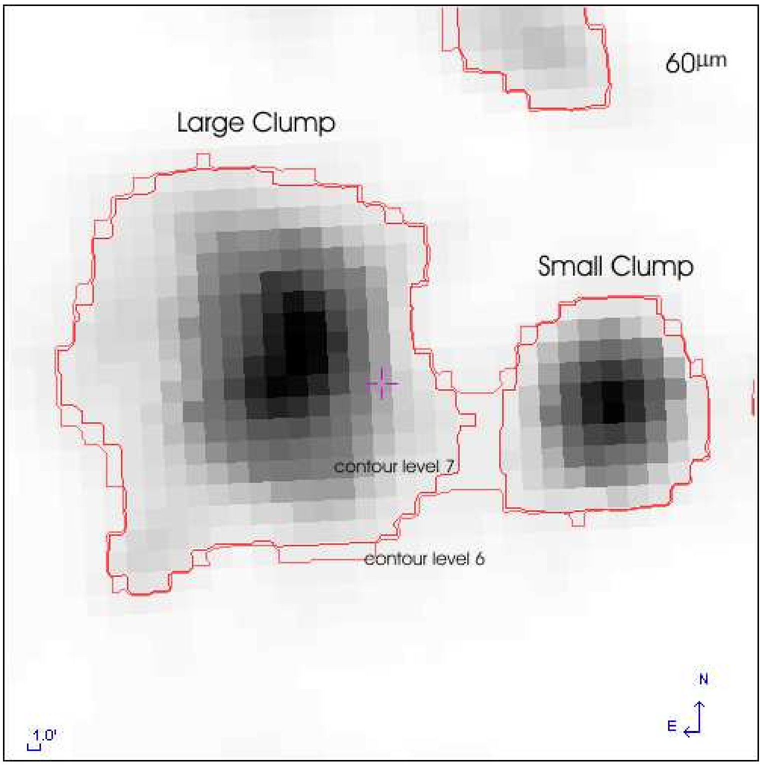


Figure 4.4: Clump separation at contour level 7 in 60 micron IRAS image.

## 4.3 Relative Flux Density

We obtained the relative flux density of each pixel using ALADIN2.5 software. Each value of the flux density and the coordinate of the pixel was noted for further calculation.

### 4.3.1 Background Correction

The obtained relative flux density by clicking on each pixel of fits image in Aladin includes flux of other objects in the background, which is also called background flux. For the correction of the background flux, we inspected the pixels with minimum flux in the entire image (of course other than the region of our interest) and obtained the average background flux. We then subtracted the background flux from all the flux density values. All the flux density values written in the dissertation are corrected flux density.

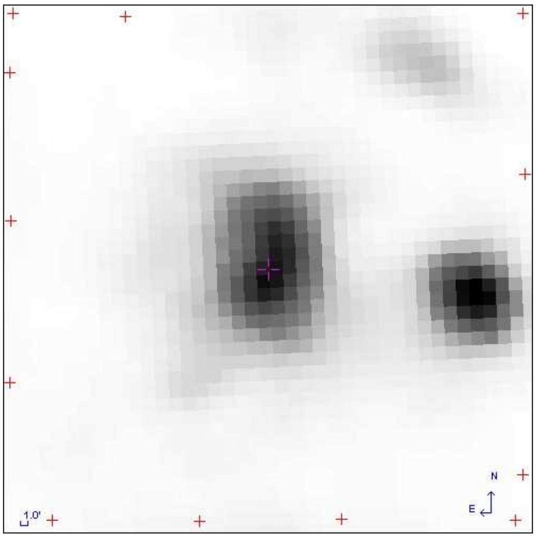


Figure 4.5: Clicks at minimum flux region to find the background correction.

## 4.4 Dust Color Temperature

To calculate the dust color temperature, we obtained the relative flux densities of each pixel at 100$\mu$m and 60 $\mu$m images. The ratio of the corrected flux densities was used to study the temperature profile of our region of interest. We used the expression given at equation (2.5) to calculate the temperature.

## 4.5 Dust Mass

Dust masses are estimated from the infrared background corrected flux densities at 100 $\mu$m image, following the analysis of Meaburn et al. (2000). The infrared flux can be measured from IRAS Sky View images and images from the Groningen using ALADIN2.5. The resulting dust mass depends on the physical and chemical properties of the dust grains, the adopted dust temperature and the distance to the object. The final expression for the dust mass can be written as:

$$M_{dust} = \frac{4}{3}\frac{a\rho}{Q_\nu}[\frac{S_\nu D^2}{B(\nu,T)}] \tag{4.1}$$

where,
$a$ = weighted grain size
$\rho$ = grain density
$Q_\nu$ = grain emissivity
$S_\nu$ = total flux density of the region whose mass is to be determined
$D$ = distance of the structure
$B(\nu,T)$ = Planck's function, which is the function of the temperature and the frequency and given by the expression:

$$B(\nu,T) = \frac{2h\nu^3}{c^2}[\frac{1}{exp(\frac{h\nu}{KT}) - 1}] \tag{4.2}$$

where,
$h$ = Planck's constant
$c$ = velocity of light
$\nu$ = frequency at which the emission is observed
$T$ = average temperature of the region
Value of different parameters we use in the calculation of the dust mass in our region of interest are as follows:
$a = 0.1$ $\mu$m (Young et al. 1993)
$\rho = 3000$ kg m$^{-3}$ (Young et al. 1993)
$Q_\nu = 0.0010$ for 100 $\mu$m and 0.0046 for 60 $\mu$m respectively (Young et al. 1993)

Using these values the expression 4.1 takes the form:

$$M_{dust} = 0.4[\frac{S_\nu D^2}{B(\nu,T)}] \tag{4.3}$$

We used equation (4.3) to calculate the mass profile of each pixel.

## 4.6 Major and Minor Diameter

We calculated the major and minor diameter of the separated clumps at different contour levels using distance tool in ALADIN2.5 software. We have used the values of the major and minor diameter to analyze the inclination angle of the molecular cloud.

We also studied the flux density variation along major and minor axis using 100 $\mu$m image.

## 4.7 Angle of Inclination

It is always possible that any molecular cloud plane is inclined by a certain angle with respect to the plane of the sky. The inclination angle i (angle between the line of sight and the normal vector of the plane of the structure) can be estimated using (Holmberg 1946),

$$\cos^2 i = \frac{(b/a) - q_*^2}{1 - q_*^2} \tag{4.4}$$

with $b/a$ as the measured axial ratio and $q_*$ as the intrinsic flatness of the structure.

We estimated the major and minor diameter of the molecular clumps with the help of ALADIN tools and calculated the values of inclination angle varying the intrinsic flatness.

# Chapter 5

# Result and Discussion

We present our result concerning the dust color temperature, dust mass, flux density variation, inclination angle of the structure and discrete sources found in the region of interest below. In order to study the infrared emission, we have used 60$\mu$m and 100$\mu$m IRAS maps obtained from Groningen IRAS server.

## 5.1 Position of Maximum Flux

At first we had a survey of the region of maximum relative flux in 100 $\mu$m and 60 $\mu$m images using ALADIN2.5 software. We noted the position and the relative flux density of these regions which are also presented in table 5.1. We found the different result in 100 $\mu$m and

Table 5.1: Maximum flux (SI units) observed in 100 micron IRAS images with their corresponding position (last column). The position (second and third column) provided here represents the pixel of maximum flux.

| Clump | R.A.(J2000) hr min sec | Dec. (J2000) deg min sec | Flux Density ($\times 10^{-25}$) |
|---|---|---|---|
| Large Clump | 11 15 13.51 | -61 17 38.9 | 9.1 |
| Small Clump | 11 11 52.81 | -61 19 25.5 | 11.3 |

Table 5.2: Maximum flux (SI units) observed in 60 micron IRAS images with their corresponding position (last column). The position (second and third column) provided here represents the pixel of maximum flux.

| Clump | R.A.(J2000) hr min sec | Dec.(J2000) deg min sec | Flux Density ($\times 10^{-25}$) |
|---|---|---|---|
| Large Clump | 11 15 01.32 | -61 15 58.7 | 9.5 |
| Small Clump | 11 11 52.80 | -61 19 28.8 | 9.0 |

60 $\mu$m image. In the larger clump (as shown in Fig.5.1) of our region of interest, maximum relative flux is higher in 60 $\mu$m image. Whereas in smaller clump, the maximum flux is higher in 100 $\mu$m image. This result indicates that the IRAS maps at 60$\mu$m and 100$\mu$m show slightly different emission feature. However the level of flux density is almost similar in both maps.

## 5.2 Dust Color Temperature

We calculated the dust color temperature of each pixel of our region of interest using the method proposed by Schnee et al. (2005). For this we use the IRAS 100 $\mu$m and 60 $\mu$m fits images downloaded from the IRAS survey. We did not select IRAS 25 $\mu$m and 12 $\mu$m images because of the insignificant emission. For the calculation of temperature we choose the value of $\beta = 2$ following the explanation given by Dupac et al. (2003).

Table 5.3: Maximum and minimum temperature (T, in Kelvin) in our region of interest (inside contour level 11 in 100 $\mu$m image)

| | R.A.(J2000) | Dec.(J2000) | R=$\frac{F(60)}{F(100)}$ | T (K) |
|---|---|---|---|---|
| Min | 11 12 01.79 | -61 27 00.6 | 0.27 | 24.80 |
| Max | 11 15 39.51 | -61 13 22 | 1.24 | 40.98 |

Inside the region of our interest (bounded by contour level 11 in IRAS 100 $\mu$m image), we found the minimum dust color temperature 24.80 K and the maximum dust color temperature is found to be 40.98 K.

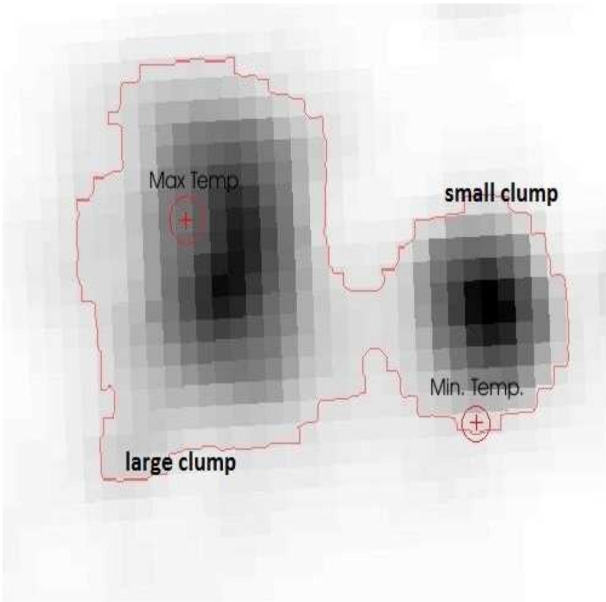


Figure 5.1: Maximum and Minimum temperature in the region inside contour level 11 drawn in IRAS 100 $\mu$m image.

Both the minimum and maximum temperature region do not lie in the central maximum flux region. The maximum temperature region lies approximately 23.97 parsec from the center of the image and 11.24 parsec from the maximum flux region in larger clump. Similarly, the minimum temperature region lies approximately 37.79 parsec from the center and 15.84 parsec from the maximum flux region in smaller clump.

## 5.3 Dust Mass

We estimated the dust mass of our region of interest following the method used by Meaburn et al. (2000) & Hildebrand (1983) (equation 4.3) using 100 $\mu$m IRAS image. The infrared flux is obtained from Groningen IRAS server available at official website of SKYVIEW virtual observatory. By using the relative flux density values of each pixel, we calculated the dust color temperature. We calculated the value of Plank function for each pixel with the help of corresponding dust color temperature. Finally the dust mass was estimated using the Plank function and the corrected flux density obtained from IRAS 100 $\mu$m image.

Assuming the ratio of mass of the gas to the dust mass as 200 (Aryal & Weinberger 2006, Aryal, Rajbahak & Weinberger 2010),we calculated the dust mass of the region of our interest. We found the total mass of the gas in the region (bounded by contour level 11 in 100 $\mu$m image) to be equal to $3.1\times10^4$ $M_\odot$. This mass is sufficiently high to check the Jean's limit.

We also studied the mass of the regions included inside contour level 12 and 100 from the same fits image as the region is separated at contour level 12 in two clumps. The dust mass obtained in different contour levels are presented in the table 5.4. From the table we clearly see that the smaller clump has higher mass, which means the smaller clump has the larger density of gas and hence it is the most probable star forming region.

Table 5.4: Table showing the calculated mass of the gas at contour level 12 and 100 using IRAS 100 $\mu$m image. The region is separated fairly at contour level 12 in large and small clumps (See Fig.4.2).

| Clump | Contour Level | Dust Mass $M_\odot$ |
|---|---|---|
| Large | 12 | $1.20\times10^4$ |
| | 100 | $0.52\times10^4$ |
| Small | 12 | $1.50\times10^4$ |
| | 100 | $0.57\times10^4$ |

## 5.4 Size of the Structure

We found the molecular cloud separates at contour level 12. After separating the cloud in two clumps, we measured the major and minor diameter for both small and large clump. The diameter of the clumps are tabulated below.

Table 5.5: Major and Minor Diameter of the clumps at contour level 12 of 100 micron image

| Clump | Major Diameter (pc) | Minor Diameter (pc) |
|---|---|---|
| Large Clump | 64.40 | 42.85 |
| Small Clump | 34.11 | 28.76 |

The size is comparable to that of size of Draco Cloud (Odenwald & Rickard, 1989) and Skeleton Nebula (Aryal & Weinberger, 2006). However the mass of these clumps of our region of interest are extremely high than that of the other clouds.

## 5.5 Flux Density Variation

We studied the flux density variation of the region along the major and minor diameter of the clumps. As the clumps are separated at contour level 12, we studied the variation of the relative flux density along the major and minor diameter of the area included by contour level 12.

Table 5.6: The Gussian fit parameters obtained from the plots of flux density variation along major and minor diameter.

| Clump | Diameter | Gussian Parameters | | | | |
|---|---|---|---|---|---|---|
| | | Area ($\times 10^5$) | Center | Width | Offset | Height |
| Small | Major | 2.75 | 0.61 | 10.79 | 1142.50 | 20417 |
| | Minor | 2.73 | -0.60 | 10.29 | 747.45 | 21155 |
| Large | Major | 3.32 | 3.27 | 16.04 | 1287.20 | 16519 |
| | Minor | 2.28 | 1.38 | 11.67 | 1430.60 | 15630 |

A gussian like distribution (See Fig. 5.3) along both the major and minor diameter strongly suggests the structure is isolated and complete in itself (Soker et al.,2002)

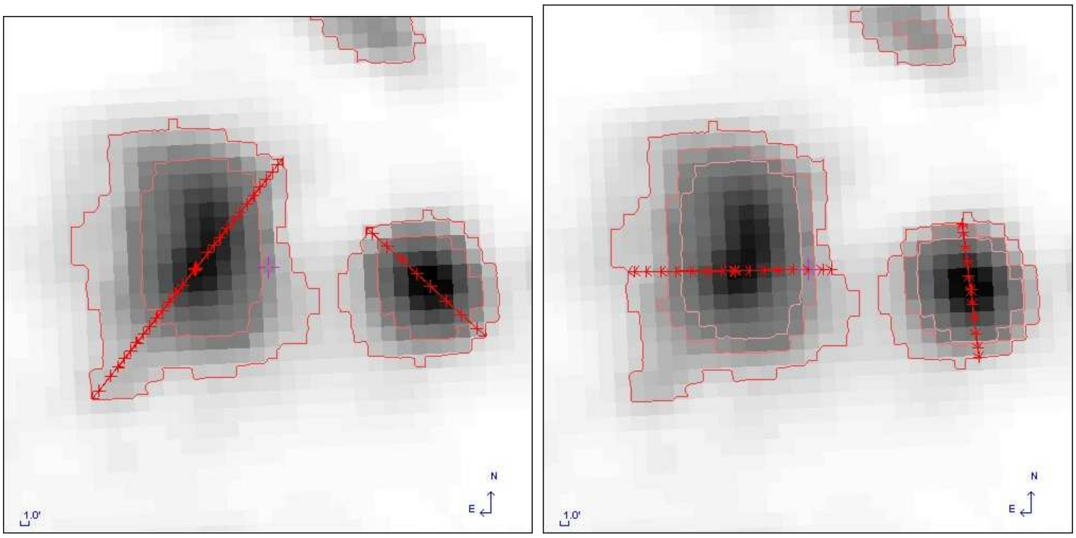

Figure 5.2: Left: The relative flux density variation along major diameter. Right: The relative flux variation along minor diameter. Note that both the diameter are drawn on contour level 12 on IRAS 100 Micron image.

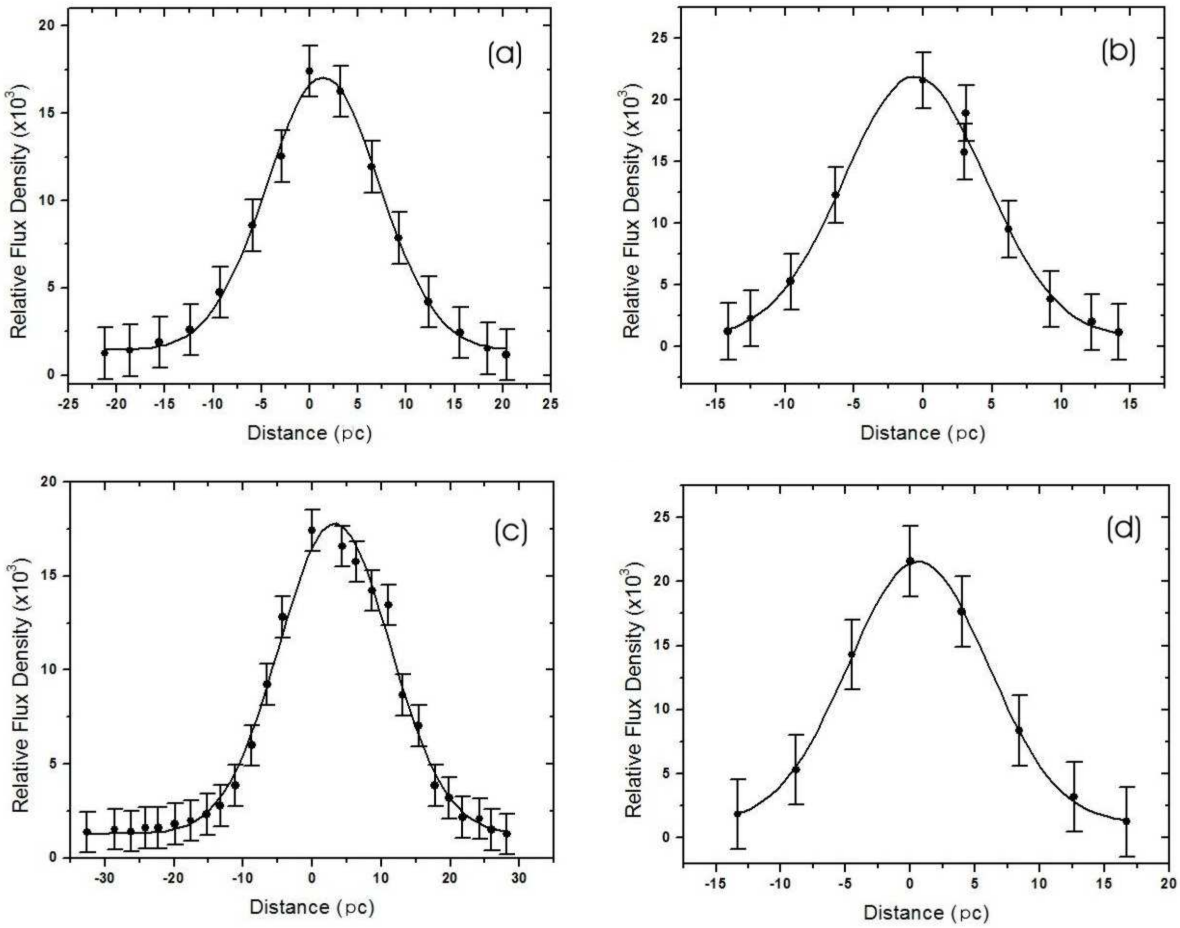


Figure 5.3: The relative flux density variation along major diameter and minor diameter. [Fig. a] and [Fig. c] represent flux variation along minor and major diameter respectively in larger clump. [Fig. b] and [Fig. d] represent flux variation along minor and major diameter respectively in smaller clump.

## 5.6 Angle of Inclination

The inclination angle ($i$) is the angle between the line of sight and the normal vector of the plane of the cometary structure. This can be estimated by using Holmborg (1946) formula,

$$\cos^2 i = \frac{(b/a) - q_*^2}{1 - q_*^2} \tag{5.1}$$

where, b/a is the ratio of minor to major diameter and $q_*$ is the intrinsic flatness of the structure. The intrinsic flatness of the interstellar cloud depends on the amount of molecular hydrogen and dust. Because of the photoelectric heating and low-energy cosmic ray heating, the grains in the dust gain energy. Because of this vibrational degrees of freedom is greatly enhanced. This makes the cloud to be flat (opening angle gradually increases with the dilution and vibrational excitation of the dust). Thus the range of the intrinsic flatness of the cloud is wide. Here we varied the intrinsic flatness from 0.20 to 0.40 for the molecular cloud.

Table 5.7 and 5.8 give the values of inclination angle for various contour levels in 60 and 100 $\mu$m maps respectively.

At the contour level 12, inclination angle of the large clump is found to be $\sim 7°$ more in 60 $\mu$m IRAS map than that of the 100 $\mu$m IRAS map. This difference is found to be reduced significantly at contour level 36. Interestingly, a similar trend is found in the smaller clump. (See Table 5.7 & 5.8). This suggests a systemetic orientation in the large as well as small clumps of the molecular cloud NGC3603. In the large clump, inclination is found to be increased by a small angle than in the small clump as seen in 100 $\mu$m. In 60 $\mu$m, inclination angle is found to be decreased with increasing contour level in the large clump whereas an opposite tendency is noticed in the small clump. This result suggests a significant difference in the orientation of contour levels in the large and small clumps.

As a while, the range of the inclination is gound to lie in between 30°-60°, suggesting neither face on (i=0°) nor edge-on (i=90°) structure. The small clump is found to be nearly face-on whereas large clump seems to be nearly face-on.

Table 5.7: Observed inclination angle using Holmborg formula and varying the value of intrinsic flatness. The major and minor diameter of small and large clump are measured at contour level 12, 24 and 36 for 60 micron IRAS image with the help of ALADIN2.5 software

| Clump | contour level level | Major Diameter (arcmin) | Minor Diameter (arcmin) | Intrinsic Flatness ($q_*$) | Inclination (deg) |
|---|---|---|---|---|---|
| | | | | 0.20 | 56.89 |
| | | | | 0.25 | 57.96 |
| Large | 12 | 29.58 | 16.91 | 0.30 | 59.36 |
| | | | | 0.35 | 61.18 |
| | | | | 0.40 | 63.57 |
| | | | | 0.20 | 54.19 |
| | | | | 0.25 | 55.15 |
| Large | 24 | 24.28 | 14.75 | 0.30 | 56.40 |
| | | | | 0.35 | 58.02 |
| | | | | 0.40 | 60.11 |
| | | | | 0.20 | 51.76 |
| | | | | 0.25 | 52.64 |
| Large | 36 | 18.94 | 12.10 | 0.30 | 53.78 |
| | | | | 0.35 | 55.23 |
| | | | | 0.40 | 57.10 |
| | | | | 0.20 | 38.04 |
| | | | | 0.25 | 38.57 |
| Small | 12 | 14.51 | 11.57 | 0.30 | 39.26 |
| | | | | 0.35 | 40.13 |
| | | | | 0.40 | 41.20 |
| | | | | 0.20 | 39.85 |
| | | | | 0.25 | 40.42 |
| Small | 24 | 12.01 | 9.35 | 0.30 | 41.16 |
| | | | | 0.35 | 42.09 |
| | | | | 0.40 | 43.24 |
| | | | | 0.20 | 43.45 |
| | | | | 0.25 | 44.11 |
| Small | 36 | 10.73 | 7.93 | 0.30 | 44.95 |
| | | | | 0.35 | 46.01 |
| | | | | 0.40 | 47.33 |

Table 5.8: Observed inclination angle using Holmborg formula and varying the value of intrinsic flatness. The major and minor diameter of small and large clump are measured at contour level 12, 24 and 26 for 100 micron IRAS image with the help of ALADIN2.5 software

| Clump | contour level | Major Diameter (arcmin) | Minor Diameter (arcmin) | Intrinsic Flatness ($q_*$) | Inclination (deg) |
|---|---|---|---|---|---|
| | | | | 0.20 | 49.66 |
| | | | | 0.25 | 50.47 |
| Large | 12 | 31.17 | 20.74 | 0.30 | 51.52 |
| | | | | 0.35 | 52.86 |
| | | | | 0.40 | 54.56 |
| | | | | 0.20 | 49.20 |
| | | | | 0.25 | 49.99 |
| Large | 24 | 22.22 | 14.91 | 0.30 | 51.03 |
| | | | | 0.35 | 52.35 |
| | | | | 0.40 | 54.02 |
| | | | | 0.20 | 51.33 |
| | | | | 0.25 | 52.19 |
| Large | 36 | 18.70 | 12.05 | 0.30 | 53.31 |
| | | | | 0.35 | 54.74 |
| | | | | 0.40 | 56.58 |
| | | | | 0.20 | 33.30 |
| | | | | 0.25 | 33.75 |
| Small | 12 | 16.51 | 13.92 | 0.30 | 34.32 |
| | | | | 0.35 | 35.05 |
| | | | | 0.40 | 35.94 |
| | | | | 0.20 | 37.22 |
| | | | | 0.25 | 37.74 |
| Small | 24 | 13.58 | 10.94 | 0.30 | 38.41 |
| | | | | 0.35 | 39.25 |
| | | | | 0.40 | 40.29 |
| | | | | 0.20 | 42.92 |
| | | | | 0.25 | 43.56 |
| Small | 36 | 12.24 | 9.12 | 0.30 | 44.38 |
| | | | | 0.35 | 45.42 |
| | | | | 0.40 | 46.72 |

## 5.7 Discrete Sources around the Center

We investigated the point sources around the maximum flux region of both the large and small clumps using SIMBAD database. We searched the objects around the maximum flux region by choosing the radius 2 arcmin. The list of the objects around the maximum flux region in large and small clumps are listed in the table 5.9 and 5.10.

Within 2 arcmin radius around the maxima of the small clump 81 stars (including cluster members), 12 Dense cores, 5 H II region, 33 IR Sources, 11 Maser objects, 7 $Y^{\star}$? (Young stellar object candidate), 4 $Y^{\star}O$ (Young Stellar Object) are found. The large number of star cluster clearly hints that the small clump might be on active star forming region.

Similarly, within 2 arcmin radius around the maxima of the small clump 41 stars, 13 star cluster members, 1 H II region, 66 IR Sources, 5 Maser objects, 10 molecular clouds are found. The large number of stars, star cluster and molecular clouds clearly advocates that the large clump might be an active star forming region.

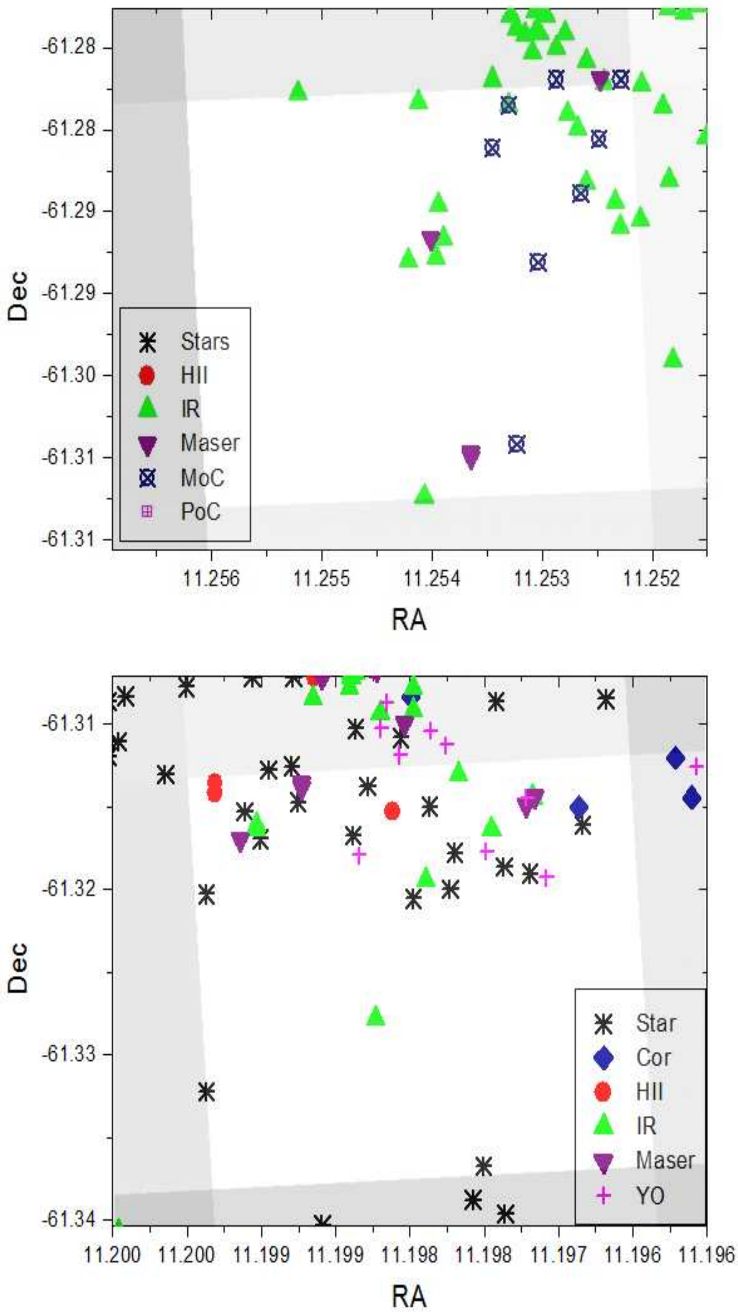


Figure 5.4: Top: The plot of the objects around the maximum flux region of large clump. Buttom: The plot of the objects around the maximum flux region of small clump.

Table 5.9: Objects around the maximum flux in smaller clump. We obtained the objects searching with 2 arcmin radious SIMBAD giving the center of the maximum flux pixel in small clump

| Identifier | Distance arcsec | OType | R.A. Hr Min Sec | Dec. Deg Min Sec | Sp. Type |
|---|---|---|---|---|---|
| Object | dist arcsec | otype | RA | Dec | sp type |
| [PRT94] 56 | 11.87 | * | 11 11 52.4 | -61 19 14 | |
| [PRT94] 53 | 16.47 | * | 11 11 51.5 | -61 19 12 | |
| [PRT94] 52 | 23.78 | * | 11 11 51.4 | -61 19 04 | |
| [PRT94] 47 | 26.37 | * | 11 11 50.2 | -61 19 07 | |
| 2MASS J11115385-6119002 | 26.38 | * | 11 11 53.85 | -61 19 00.2 | |
| 2MASS J11114957-6119085 | 28.8 | * | 11 11 49.58 | -61 19 08.5 | |
| [PRT94] 55 | 32.04 | * | 11 11 52.0 | -61 18 54 | |
| [MBW2006] 230 | 34.08 | * | 11 11 56.1 | -61 19 01 | |
| [PRT94] 80 | 35.33 | * | 11 11 57.4 | -61 19 13 | |
| 2MASS J11115349-6118494 | 36.34 | * | 11 11 53.50 | -61 18 49.5 | |
| [PRT94] 70 | 36.77 | * | 11 11 55.2 | -61 18 53 | |
| 2MASS J11115647-6118550 | 40.35 | * | 11 11 56.48 | -61 18 55.0 | |
| [PRT94] 42 | 42.55 | * | 11 11 48.3 | -61 18 58 | |
| 2MASS J11115534-6118451 | 44.22 | * | 11 11 55.34 | -61 18 45.2 | |
| [PRT94] 82 | 44.96 | * | 11 11 57.4 | -61 19 56 | |
| [PRT94] 74 | 45.33 | * | 11 11 55.9 | -61 18 46 | |
| [PRT94] 57 | 46.51 | * | 11 11 52.7 | -61 18 39 | |
| [PRT94] 58 | 49.02 | * | 11 11 53.8 | -61 18 37 | |
| 2MASS J11115069-6120122 | 49.11 | * | 11 11 50.70 | -61 20 12.2 | |
| 2MASS J11115095-6120195 | 55.63 | * | 11 11 50.95 | -61 20 19.5 | |
| [PRT94] 86 | 55.69 | * | 11 11 58.4 | -61 18 47 | |
| [PRT94] 39 | 55.89 | * | 11 11 46.7 | -61 20 00 | |
| [PRT94] 48 | 57.2 | * | 11 11 50.4 | -61 18 31 | |
| 2MASS J11115016-6120225 | 60.18 | * | 11 11 50.17 | -61 20 22.6 | |
| [PRT94] 67 | 60.88 | * | 11 11 54.6 | -61 20 25 | |
| [MBW2006] 229 | 62.14 | * | 11 11 55.3 | -61 18 26 | |
| 2MASS J11115320-6118224 | 63.17 | * | 11 11 53.21 | -61 18 22.4 | |
| [PRT94] 99 | 64.46 | * | 11 12 01.3 | -61 19 05 | |
| [PRT94] 75 | 64.59 | * | 11 11 56.3 | -61 18 26 | |
| [PRT94] 93 | 65.87 | * | 11 11 59.8 | -61 18 43 | |
| 2MASS J11114773-6118306 | 65.97 | * | 11 11 47.73 | -61 18 30.6 | |
| 2MASS J11115954-6118398 | 66.66 | * | 11 11 59.55 | -61 18 39.8 | |
| [PRT94] 85 | 68.19 | * | 11 11 57.9 | -61 18 28 | |
| 2MASS J11114309-6119063 | 72.56 | * | 11 11 43.09 | -61 19 06.3 | |
| HD 306206 | 72.92 | * | 11 11 59.375 | -61 18 29.97 | B0V |
| 2MASS J11120277-6119406 | 73.35 | * | 11 12 02.78 | -61 19 40.7 | |
| [PRT94] 92 | 74.18 | * | 11 11 59.8 | -61 18 31 | |
| 2MASS J11114239-6119233 | 75.03 | * | 11 11 42.39 | -61 19 23.4 | |
| 2MASS J11114396-6118427 | 76.75 | * | 11 11 43.96 | -61 18 42.7 | |
| 2MASS J11115707-6118130 | 78.63 | * | 11 11 57.07 | -61 18 13.1 | |
| [PRT94] 95 | 78.95 | * | 11 12 01.0 | -61 18 33 | |
| 2MASS J11120382-6119303 | 79.46 | * | 11 12 03.83 | -61 19 30.3 | |
| 2MASS J11115348-6118045 | 81.14 | * | 11 11 53.48 | -61 18 04.5 | |
| 2MASS J11120074-6118260 | 82.46 | * | 11 12 00.74 | -61 18 26.0 | |
| [PRT94] 91 | 82.92 | * | 11 11 59.5 | -61 18 18 | |
| 2MASS J11114255-6118465 | 83.53 | * | 11 11 42.55 | -61 18 46.5 | |
| 2MASS J11115652-6118062 | 83.58 | * | 11 11 56.52 | -61 18 06.3 | |
| [PRT94] 103 | 83.81 | * | 11 12 02.1 | -61 18 35 | |
| [PRT94] 63 | 86 | * | 11 11 54.1 | -61 18 00 | |
| 2MASS J11120391-6119579 | 86.21 | * | 11 12 03.91 | -61 19 57.9 | |
| 2MASS J11114083-6119313 | 86.42 | * | 11 11 40.83 | -61 19 31.3 | |
| 2MASS J11115826-6118065 | 88.15 | * | 11 11 58.27 | -61 18 06.6 | |
| 2MASS J11115700-6118019 | 88.78 | * | 11 11 57.00 | -61 18 02.0 | |
| [PRT94] 73 | 90.28 | * | 11 11 55.9 | -61 17 58 | |
| [PRT94] 41 | 91.21 | * | 11 11 48.4 | -61 18 00 | |
| 2MASS J11114099-6119595 | 91.58 | * | 11 11 41.00 | -61 19 59.6 | |
| [PRT94] 36 | 91.63 | * | 11 11 45.4 | -61 18 11 | |
| [PRT94] 87 | 94.23 | * | 11 11 58.6 | -61 18 01 | |
| [PRT94] 97 | 95.14 | * | 11 12 01.2 | -61 18 12 | |
| [PRT94] 37 | 96.23 | * | 11 11 45.7 | -61 20 47 | |
| [PRT94] 100 | 98.68 | * | 11 12 01.3 | -61 20 43 | |
| [PRT94] 38 | 100.13 | * | 11 11 45.8 | -61 20 52 | |
| [PRT94] 72 | 100.83 | * | 11 11 55.8 | -61 17 47 | |
| [PRT94] 59 | 101.75 | * | 11 11 53.8 | -61 17 44 | |
| 2MASS J11114094-6120221 | 102.41 | * | 11 11 40.95 | -61 20 22.1 | |
| [PRT94] 81 | 102.95 | * | 11 11 57.4 | -61 17 48 | |
| 2MASS J11115869-6117511 | 103.46 | * | 11 11 58.69 | -61 17 51.1 | |
| [PRT94] 105 | 103.56 | * | 11 12 02.8 | -61 18 11 | |
| [PRT94] 21 | 103.89 | * | 11 11 38.5 | -61 19 12 | |
| [PRT94] 94 | 104.29 | * | 11 12 00.9 | -61 17 59 | |
| [PRT94] 113 | 105.3 | * | 11 12 06.0 | -61 18 40 | |
| [PRT94] 17 | 106.94 | * | 11 11 38.0 | -61 19 17 | |
| 2MASS J11113807-6119043 | 108.2 | * | 11 11 38.07 | -61 19 04.3 | |
| [PRT94] 107 | 109.44 | * | 11 12 03.4 | -61 18 07 | |
| 2MASS J11120403-6118111 | 109.81 | * | 11 12 04.04 | -61 18 11.2 | |
| [PRT94] 26 | 109.84 | * | 11 11 41.6 | -61 18 11 | |
| [PRT94] 15 | 111.19 | * | 11 11 37.6 | -61 19 45 | |
| [PRT94] 96 | 112.16 | * | 11 12 01.2 | -61 17 51 | |
| [PRT94] 14 | 119.89 | * | 11 11 36.6 | -61 18 58 | |
| [R2003] 338 | 98.32 | ? | 11 12.1 | -61 19 | |
| NAME NGC 3576 IR CLUSTER | 57.7 | Cl* | 11 11 55 | -61 18.5 | |

contd..

| Identifier | Distance arcsec | OType | R.A. Hr Min Sec | Dec. Deg Min Sec | Sp. Type |
|---|---|---|---|---|---|
| [$PML$2009] 10 | 44.7 | cor | 11 11 48.39 | -61 18 54.1 | |
| [$PML$2009] 8 | 55.36 | cor | 11 11 52.45 | -61 18 30.2 | |
| [$PML$2009] 12 | 61.41 | cor | 11 11 45.66 | -61 18 52.0 | |
| [$PML$2009] 9 | 63.63 | cor | 11 11 51.91 | -61 18 22.2 | |
| [$PML$2009] 11 | 64.35 | cor | 11 11 46.05 | -61 18 43.4 | |
| [$PML$2009] 7 | 68.25 | cor | 11 12 01.53 | -61 18 58.7 | |
| [$PML$2009] 13 | 79.12 | cor | 11 11 41.86 | -61 19 32.4 | |
| [$PML$2009] 5 | 96.6 | cor | 11 12 05.25 | -61 18 49.3 | |
| [$PML$2009] 14 | 98.45 | cor | 11 11 39.38 | -61 19 44.2 | |
| [$PML$2009] 6 | 105.29 | cor | 11 12 04.76 | -61 18 24.8 | |
| [$PML$2009] 18 | 107.6 | cor | 11 11 37.92 | -61 19 35.1 | |
| [$PML$2009] 15 | 111.94 | cor | 11 11 38.90 | -61 20 15.6 | |
| GAL 291.3-00.7 | 30.51 | HII | 11 11 52.9 | -61 18 55 | |
| OH 291.3 -0.7 | 46.79 | HII | 11 11 57.2 | -61 18 51 | |
| NGC 3581 | 48.28 | HII | 11 11 57.2 | -61 18 49 | |
| NAME NGC 3576 IRS 1 | 61.2 | HII | 11 11 54.8 | -61 18 26 | |
| NGC 3576 | 74.71 | HII | 11 11 49.8 | -61 18 14 | |
| 2MASS J11115331-6119402 | 15.15 | IR | 11 11 53.32 | -61 19 40.2 | |
| [$MS$81] 291.27-0.71 IRS 1 | 16.32 | IR | 11 11 52.1 | -61 19 10 | |
| MSX6C G291.2725-00.7198 | 31.29 | IR | 11 11 50.5 | -61 18 59 | |
| [$BE$83] IR 291.28-00.71 | 36.02 | IR | 11 11 56.2 | -61 18 59 | |
| [$MS$81] 291.27-0.71 IRS 3 | 36.77 | IR | 11 11 56.2 | -61 18 58 | |
| [$WBB$2001] 17 | 40.01 | IR | 11 11 51.3 | -61 18 47 | |
| [$WBB$2001] 18 | 41.11 | IR | 11 11 49.5 | -61 18 52 | |
| [$MBW$2006] 227 | 51.98 | IR | 11 11 53.20 | -61 18 33.6 | |
| MSX5C G291.2732-00.7115 | 52.58 | IR | 11 11 52.4 | -61 18 33 | |
| 2MASS J11115483-6118305 | 56.81 | IR | 11 11 54.84 | -61 18 30.6 | |
| [$MBW$2006] 226 | 57.38 | IR | 11 11 52.40 | -61 18 28.2 | |
| 2MASS J11115393-6118282 | 57.78 | IR | 11 11 53.94 | -61 18 28.3 | |
| [$BE$83] IR 291.27-00.71 | 60.02 | IR | 11 11 53.9 | -61 18 26 | |
| NAME RCW 57 IRS 1 | 60.92 | IR | 11 11 53.8 | -61 18 25 | |
| [$MS$81] 291.27-0.71 IRS 2 | 61.01 | IR | 11 11 53.9 | -61 18 25 | |
| 2MASS J11115437-6118240 | 62.53 | IR | 11 11 54.38 | -61 18 24.0 | |
| 2MASS J11120157-6119166 | 63.67 | IR | 11 12 01.57 | -61 19 16.7 | |
| 2MASS J11115180-6118204 | 65.5 | IR | 11 11 51.80 | -61 18 20.4 | |
| [$WBB$2001] 16 | 67.5 | IR | 11 11 52.9 | -61 18 18 | |
| 2MASS J11114317-6119156 | 70.09 | IR | 11 11 43.17 | -61 19 15.6 | |
| 2MASS J11115107-6118143 | 72.29 | IR | 11 11 51.07 | -61 18 14.3 | |
| 2MASS J11115953-6120266 | 77.92 | IR | 11 11 59.53 | -61 20 26.6 | |
| 2MASS J11114314-6118392 | 83.55 | IR | 11 11 43.15 | -61 18 39.2 | |
| [$MBW$2006] 212 | 83.95 | IR | 11 12 01.8 | -61 20 19 | |
| [$MBW$2006] 231 | 86.14 | IR | 11 12 04.4 | -61 19 47 | |
| 2MASS J11114766-6120444 | 87.23 | IR | 11 11 47.67 | -61 20 44.5 | |
| 2MASS J11120567-6119349 | 93.05 | IR | 11 12 05.67 | -61 19 35.0 | |
| 2MASS J11113967-6119300 | 94.62 | IR | 11 11 39.68 | -61 19 30.1 | |
| [$MBW$2006] 233 | 99.32 | IR | 11 12 06.6 | -61 19 29 | |
| 2MASS J11114251-6118156 | 101.91 | IR | 11 11 42.51 | -61 18 15.6 | |
| [$MBW$2006] 232 | 105.51 | IR | 11 12 05.6 | -61 18 34 | |
| [$MBW$2006] 225 | 109.54 | IR | 11 11 52.4 | -61 21 15 | |
| [$MBW$2006] 234 | 110.07 | IR | 11 12 08.1 | -61 19 27 | |
| Caswell H2O 291.28-00.71 | 36.5 | Mas | 11 11 56.58 | -61 19 01.1 | |
| Caswell H2O 291.27-00.72 | 38.93 | Mas | 11 11 49.67 | -61 18 53.8 | |
| [$BE$83] Maser 291.28-00.71 | 39.14 | Mas | 11 11 55.1 | -61 18 50 | |
| [$HLB$98] SEST 48 | 40.05 | Mas | 11 11 55.1 | -61 18 49 | |
| Caswell CH3OH 291.270-00.719 | 41.44 | Mas | 11 11 49.44 | -61 18 51.9 | |
| [$HLB$98] SEST 47 | 49.52 | Mas | 11 11 52.6 | -61 18 36 | |
| Caswell CH3OH 291.28-00.71 | 60.88 | Mas | 11 11 54.6 | -61 18 26 | |
| Caswell H2O 291.27-00.71 | 61.49 | Mas | 11 11 53.28 | -61 18 24.1 | |
| Caswell CH3OH 291.274-00.709 | 61.92 | Mas | 11 11 53.35 | -61 18 23.7 | |
| Caswell OH 291.274-00.709 | 62.27 | Mas | 11 11 53.44 | -61 18 23.4 | |
| [$GVS$2000] 11097-6102 | 92.25 | Mas | 11 11.8 | -61 18 | |
| [$HBM$2005] G291.27-0.70 | 61.2 | mm | 11 11 54.8 | -61 18 26 | |
| [$HBM$2005] G291.288-0.706 | 76.14 | mm | 11 12 00.6 | -61 18 34 | |
| [$HBM$2005] G291.256-0.743 | 108.25 | mm | 11 11 38.3 | -61 19 54 | |
| Kes 14 | 105.96 | Rad | 11 12 03 | -61 20.7 | |
| 2MASS J11115370-6119044 | 21.98 | Y*? | 11 11 53.71 | -61 19 04.5 | |
| [$MHL$2007] G291.2725-00.7198 1 | 26.9 | Y*? | 11 11 50.62 | -61 19 03.7 | |
| [$MHL$2007] G291.2725-00.7198 2 | 30.69 | Y*? | 11 11 49.18 | -61 19 09.4 | |
| [$MHL$2007] G291.2725-00.7198 4 | 42.8 | Y*? | 11 11 52.72 | -61 18 42.7 | |
| [$MHL$2007] G291.2725-00.7198 3 | 45.74 | Y*? | 11 11 51.60 | -61 18 40.6 | |
| 2MASS J11115198-6118374 | 48.47 | Y*? | 11 11 51.98 | -61 18 37.4 | |
| [$MHL$2007] G291.2725-00.7198 7 | 48.67 | Y*? | 11 11 53.18 | -61 18 36.9 | |
| [$AMG$2008] S3-M5 | 40.49 | Y*O | 11 11 49.65 | -61 18 52.0 | |
| [$AMG$2008] S3-M4 | 54.16 | Y*O | 11 11 53.050 | -61 18 31.37 | |
| [$AMG$2008] S3-C3 | 66.01 | Y*O | 11 11 45.540 | -61 18 45.27 | |
| [$AMG$2008] S4-M6 | 96.07 | Y*O | 11 11 39.690 | -61 19 43.18 | |
| GAL 291.29-00.72 | 41.51 | | 11 11 57.9 | -61 19 06 | |

Table 5.10: Objects around the maximum flux in largere clump. We obtained the objects searching with 2 arcmin radious SIMBAD giving the center of the maximum flux pixel in large clump

| Identifier | Distance arcsec | OType | R.A. Hr Min Sec | Dec. Deg Min Sec | Sp. Type |
|---|---|---|---|---|---|
| 2MASSJ11151371 − 6117434 | 4.82 | * | 11 15 13.71 | -61 17 43.5 | |
| 2MASSJ11151637 − 6117096 | 35.74 | * | 11 15 16.37 | -61 17 09.7 | |
| 2MASSJ11150821 − 6118066 | 47.23 | * | 11 15 08.21 | -61 18 06.7 | |
| 2MASSJ11151972 − 6118124 | 55.89 | * | 11 15 19.72 | -61 18 12.4 | |
| [SB2004]56746 | 61.93 | * | 11 15 10.61 | -61 16 40.6 | |
| [SB2004]56599 | 73.8 | * | 11 15 08.41 | -61 16 34.9 | |
| [SB2004]1369 | 74.83 | * | 11 15 11.88 | -61 16 25.0 | |
| [SB2004]1149 | 81.69 | * | 11 15 02.40 | -61 17 22.6 | |
| [SB2004]57235 | 85.01 | * | 11 15 17.00 | -61 16 17.7 | |
| [SB2004]57487 | 88.78 | * | 11 15 20.66 | -61 16 26.6 | |
| [SB2004]56309 | 89.5 | * | 11 15 04.22 | -61 16 39.5 | |
| [SB2004]57787 | 91.27 | * | 11 15 25.02 | -61 17 00.8 | |
| 2MASSJ11152613 − 6118062 | 94.92 | * | 11 15 26.13 | -61 18 06.2 | |
| [SB2004]57169 | 95.7 | * | 11 15 16.21 | -61 16 05.2 | |
| CPD − 602736 | 96.06 | * | 11 15 26.780 | -61 17 48.29 | |
| [SB2004]56961 | 100.22 | * | 11 15 13.24 | -61 15 58.7 | |
| [SB2004]1398 | 100.64 | * | 11 15 13.89 | -61 15 58.3 | |
| [SB2004]57101 | 104.62 | * | 11 15 15.21 | -61 15 55.0 | |
| [SB2004]58013 | 110.98 | * | 11 15 28.21 | -61 18 12.1 | |
| [SB2004]10757 | 111.01 | * | 11 15 07.94 | -61 15 55.4 | |
| [SB2004]10833 | 111.4 | * | 11 15 08.31 | -61 15 54.0 | |
| [SB2004]1141 | 111.48 | * | 11 15 01.76 | -61 16 26.4 | |
| [SB2004]10863 | 111.84 | * | 11 15 08.40 | -61 15 53.3 | |
| [SB2004]56960 | 112.82 | * | 11 15 13.24 | -61 15 46.1 | |
| [SB2004]56216 | 112.96 | * | 11 15 02.97 | -61 16 15.3 | |
| [SB2004]56366 | 116.33 | * | 11 15 05.08 | -61 15 59.7 | |
| [HEM2008]195 | 116.46 | * | 11 15 07.64 | -61 15 50.4 | |
| [HEM2008]199 | 116.49 | * | 11 15 07.42 | -61 15 51.0 | |
| [HEM2008]243 | 116.74 | * | 11 15 07.71 | -61 15 49.9 | |
| [SB2004]11052 | 116.91 | * | 11 15 09.25 | -61 15 46.1 | |
| [SB2004]10947 | 117.12 | * | 11 15 08.76 | -61 15 46.9 | |
| [SB2004]10964 | 117.22 | * | 11 15 08.80 | -61 15 46.7 | |
| [HEM2008]156 | 117.64 | * | 11 15 08.56 | -61 15 46.8 | |
| [SB2004]10951 | 117.86 | * | 11 15 08.77 | -61 15 46.1 | |
| [HEM2008]169 | 118.05 | * | 11 15 08.42 | -61 15 46.7 | |
| [SB2004]1294 | 118.17 | * | 11 15 08.20 | -61 15 47.1 | |
| [HEM2008]223 | 118.85 | * | 11 15 08.40 | -61 15 45.9 | |
| [SB2004]10506 | 118.99 | * | 11 15 07.15 | -61 15 49.1 | |
| [HEM2008]171 | 119.05 | * | 11 15 07.33 | -61 15 48.5 | |
| [HEM2008]95 | 119.06 | * | 11 15 07.68 | -61 15 47.5 | |
| [HEM2008]209 | 119.23 | * | 11 15 08.62 | -61 15 45.0 | |
| Cl ∗ NGC3603MTT58 | 61.55 | *iC | 11 15 07.58 | -61 16 54.6 | |
| Cl ∗ NGC3603MTT122 | 64.52 | *iC | 11 15 09.45 | -61 16 41.4 | |
| Cl ∗ NGC3603SHER47 | 101.36 | *iC | 11 15 09.353 | -61 16 02.07 | O4V |
| Cl ∗ NGC3603MTT25 | 104.51 | *iC | 11 15 11.31 | -61 15 55.6 | O3V |
| Cl ∗ NGC3603SHER18 | 104.97 | *iC | 11 15 08.71 | -61 15 59.8 | O6Iab: |
| Cl ∗ NGC3603MDS63 | 113.7 | *iC | 11 15 07.148 | -61 15 54.86 | O8.5V |
| Cl ∗ NGC3603MDS6 | 117.69 | *iC | 11 15 08.9 | -61 15 46 | |
| Cl ∗ NGC3603MDS22 | 117.89 | *iC | 11 15 08.20 | -61 15 47.4 | O5III(f) |
| Cl ∗ NGC3603MDS13 | 118.46 | *iC | 11 15 08.76 | -61 15 45.5 | |
| Cl ∗ NGC3603MDS72 | 118.66 | *iC | 11 15 07.62 | -61 15 48.1 | |
| Cl ∗ NGC3603MDS12 | 119.44 | *iC | 11 15 08.70 | -61 15 44.6 | |
| Cl ∗ NGC3603MTT30 | 119.55 | *iC | 11 15 08.699 | -61 15 44.49 | O8 |
| Cl ∗ NGC3603MDS71 | 119.77 | *iC | 11 15 07.77 | -61 15 46.5 | |
| 2MASXJ11151028 − 6117368 | 23.31 | G | 11 15 10.287 | -61 17 36.88 | |
| 2MASXJ11151056 − 6116197 | 81.9 | G | 11 15 10.569 | -61 16 19.79 | |
| NGC3603 | 87.85 | HII | 11 15 09.1 | -61 16 17 | |
| [TBP2001]J111514.5 − 611735 | 7.19 | IR | 11 15 14.24 | -61 17 34.0 | |
| [TBP2001]J111514.0 − 611730 | 9.57 | IR | 11 15 14.0 | -61 17 30 | |
| 2MASSJ11151515 − 6117349 | 12.54 | IR | 11 15 15.16 | -61 17 34.9 | |
| 2MASSJ11151416 − 6117226 | 16.98 | IR | 11 15 14.17 | -61 17 22.6 | |
| [NS2003]43 | 36.89 | IR | 11 15 09.32 | -61 17 17.7 | |
| [NS2003]45B | 39.85 | IR | 11 15 08.21 | -61 17 27.5 | |
| [NS2003]36 | 40.01 | IR | 11 15 14.81 | -61 17 00.0 | |
| [NS2003]37 | 40.08 | IR | 11 15 11.87 | -61 17 00.6 | |
| [NS2003]44 | 40.58 | IR | 11 15 08.39 | -61 17 22.0 | |
| [NS2003]39B | 43.42 | IR | 11 15 09.61 | -61 17 05.8 | |
| [NS2003]39A | 44.53 | IR | 11 15 09.93 | -61 17 02.6 | |
| [TBP2001]J111512.4 − 611655 | 44.62 | IR | 11 15 12.4 | -61 16 55 | |

contd.

| Identifier | Distance arcsec | OType | R.A. Hr Min Sec | Dec. Deg Min Sec | Sp. Type |
|---|---|---|---|---|---|
| $[NS2003]45A$ | 44.9 | IR | 11 15 07.55 | -61 17 25.8 | |
| $[NS2003]47$ | 48.48 | IR | 11 15 14.63 | -61 18 26.7 | |
| $[TBP2001]J111511.1-611649$ | 52.84 | IR | 11 15 11.1 | -61 16 49 | |
| $[NS2003]12$ | 53.58 | IR | 11 15 06.50 | -61 17 56.8 | |
| $2MASSJ11150660-6117171$ | 54.25 | IR | 11 15 06.61 | -61 17 17.2 | |
| $[TBP2001]J111509.3-611651$ | 55.12 | IR | 11 15 08.76 | -61 16 55.7 | |
| $[TBP2001]J111517.8-611651$ | 55.59 | IR | 11 15 18.75 | -61 16 58.1 | |
| $[TBP2001]J111510.3-611648$ | 55.91 | IR | 11 15 10.3 | -61 16 48 | |
| $[FPA77]NGC3603IRS9A$ | 55.93 | IR | 11 15 11.34 | -61 16 45.2 | |
| $[TBP2001]J111511.6-611644$ | 56.6 | IR | 11 15 11.6 | -61 16 44 | |
| $[NS2003]34$ | 56.62 | IR | 11 15 09.32 | -61 16 51.0 | |
| $[TBP2001]J111511.0-611645$ | 56.85 | IR | 11 15 11.0 | -61 16 45 | |
| $[FPA77]NGC3603IRS9C$ | 57.28 | IR | 11 15 10.86 | -61 16 44.9 | |
| $[TBP2001]J111511.8-611641$ | 59.2 | IR | 11 15 11.8 | -61 16 41 | |
| $[TBP2001]J111510.0-611645$ | 59.54 | IR | 11 15 10.0 | -61 16 45 | |
| $[NS2003]35A$ | 60.77 | IR | 11 15 07.51 | -61 16 56.2 | |
| $2MASSJ11150682-6117011$ | 61.2 | IR | 11 15 06.83 | -61 17 01.1 | |
| $[TBP2001]J111510.7-611641$ | 61.34 | IR | 11 15 10.7 | -61 16 41 | |
| $[FPA77]NGC3603IRS9B$ | 61.44 | IR | 11 15 10.62 | -61 16 41.1 | |
| $[TBP2001]J111511.0-611640$ | 61.61 | IR | 11 15 11.0 | -61 16 40 | |
| $[TBP2001]J111514.0-611634$ | 65 | IR | 11 15 14.0 | -61 16 34 | |
| $[TBP2001]J111510.3-611637$ | 66.08 | IR | 11 15 10.3 | -61 16 37 | |
| $[TBP2001]J111504.6-611723$ | 66.14 | IR | 11 15 04.6 | -61 17 23 | |
| $[NS2003]40$ | 66.2 | IR | 11 15 05.40 | -61 17 07.8 | |
| $[NS2003]6R$ | 73.83 | IR | 11 15 16.01 | -61 16 27.3 | |
| $[TBP2001]J111517.0-611629$ | 74.29 | IR | 11 15 17.0 | -61 16 29 | |
| $[NS2003]46$ | 74.35 | IR | 11 15 05.08 | -61 18 21.8 | |
| $[NS2003]6Q$ | 74.46 | IR | 11 15 12.25 | -61 16 25.0 | |
| $[NS2003]38$ | 75.32 | IR | 11 15 04.51 | -61 17 00.6 | |
| $[NS2003]41$ | 75.69 | IR | 11 15 03.58 | -61 17 14.2 | |
| $[TBP2001]J111515.3-611623$ | 76.99 | IR | 11 15 15.3 | -61 16 23 | |
| $[NS2003]32B$ | 77.36 | IR | 11 15 06.65 | -61 16 39.4 | |
| $[TBP2001]J111505.3-611638$ | 78.99 | IR | 11 15 06.13 | -61 16 40.5 | |
| $2MASSJ11151248-6116200$ | 79.24 | IR | 11 15 12.49 | -61 16 20.0 | |
| $[TBP2001]J111507.1-611633$ | 80.48 | IR | 11 15 07.1 | -61 16 33 | |
| $[NS2003]32A$ | 82.44 | IR | 11 15 05.68 | -61 16 38.8 | |
| $[TBP2001]J111517.1-611618$ | 84.94 | IR | 11 15 17.1 | -61 16 18 | |
| $[TBP2001]J111510.4-611613$ | 88.78 | IR | 11 15 10.4 | -61 16 13 | |
| $[NS2003]29$ | 89.2 | IR | 11 15 12.91 | -61 16 09.8 | |
| $[TBP2001]J111510.1-611612$ | 90.31 | IR | 11 15 10.1 | -61 16 12 | |
| $[NS2003]33$ | 92.72 | IR | 11 15 03.46 | -61 16 41.0 | |
| $[NS2003]28$ | 95.35 | IR | 11 15 16.10 | -61 16 05.4 | |
| $[NS2003]30$ | 98.23 | IR | 11 15 05.19 | -61 16 21.1 | |
| $[NS2003]25$ | 98.35 | IR | 11 15 11.02 | -61 16 02.2 | |
| $[TBP2001]J111507.2-611610$ | 99.86 | IR | 11 15 07.2 | -61 16 10 | |
| $[NS2003]27$ | 100.1 | IR | 11 15 09.77 | -61 16 02.5 | |
| $[TBP2001]J111512.4-611557$ | 102.21 | IR | 11 15 12.4 | -61 15 57 | |
| $[NS2003]31$ | 103.04 | IR | 11 15 02.98 | -61 16 29.2 | |
| $2MASSJ11150210-6116347$ | 104.2 | IR | 11 15 02.11 | -61 16 34.8 | |
| $[NS2003]26A$ | 105.28 | IR | 11 15 07.67 | -61 16 02.4 | |
| $[TBP2001]J111503.0-611616$ | 112.3 | IR | 11 15 03.0 | -61 16 16 | |
| $[NS2003]6P$ | 112.86 | IR | 11 15 08.70 | -61 15 51.5 | |
| $[NS2003]22$ | 117.55 | IR | 11 15 05.60 | -61 15 56.1 | |
| $[NS2003]24$ | 119.64 | IR | 11 15 04.19 | -61 15 59.9 | |
| $CaswellH2O291.64-00.55$ | 10.97 | Mas | 11 15 14.4 | -61 17 30 | |
| $[HLB98]SEST50$ | 38.21 | Mas | 11 15 13.1 | -61 18 17 | |
| $[BE83]Maser291.64-00.56$ | 39.21 | Mas | 11 15 13.1 | -61 18 18 | |
| $CaswellH2O291.629-00.541$ | 55.3 | Mas | 11 15 08.88 | -61 16 54.8 | |
| $CaswellH2O291.63-00.53$ | 89.48 | Mas | 11 15 10.18 | -61 16 12.7 | |
| $[HBM2005]G291.630-0.545$ | 45.37 | mm | 11 15 08.9 | -61 17 08 | |
| $[NBY2002]MM2C$ | 19.2 | MoC | 11 15 10.9 | -61 17 35 | |
| $[NBY2002]MM2B$ | 29.99 | MoC | 11 15 12.4 | -61 17 10 | |
| $[NBY2002]MM2D$ | 34.53 | MoC | 11 15 09.5 | -61 17 20 | |
| $[NBY2002]MM3B$ | 38.63 | MoC | 11 15 11.6 | -61 18 15 | |
| $[NBY2002]MM2$ | 40.08 | MoC | 11 15 11.87 | -61 17 00.6 | |
| $[NBY2002]MM2A$ | 49.62 | MoC | 11 15 10.3 | -61 16 55 | |
| $[NBY2002]MM2E$ | 58.24 | MoC | 11 15 08.2 | -61 16 55 | |
| $[NBY2002]MM2F$ | 88.74 | MoC | 11 15 09.5 | -61 16 15 | |
| $[NBY2002]MM3$ | 106.72 | MoC | 11 15 15.1 | -61 19 25 | |
| $[NBY2002]MM14$ | 116.96 | MoC | 11 15 17.2 | -61 15 45 | |
| $[TBP2001]J111516.3-611606$ | 95.05 | PoC | 11 15 16.3 | -61 16 06 | |
| $[TBP2001]J111513.1-611552$ | 106.94 | PoC | 11 15 13.1 | -61 15 52 | |
| $[CMS2009]G291.632-00.540$ | 48.41 | PoG | 11 15 11 | -61 16.9 | |
| $GRS291.63-00.54$ | 61.16 | Rad | 11 15 09.5 | -61 16 45 | |
| $Kes15$ | 118.04 | Rad | 11 15 06 | -61 15.9 | |
| $[SB2004]X10$ | 29.78 | X | 11 15 15.92 | -61 18 03.1 | |
| $[SB2004]X9$ | 39.16 | X | 11 15 15.29 | -61 17 01.9 | |
| $[SB2004]X8$ | 44 | X | 11 15 12.35 | -61 16 55.7 | |
| $[SB2004]X11$ | 109.11 | X | 11 15 22.72 | -61 16 12.3 | |
| $EQ1112-6100$ | 82.57 | | 11 15 03 | -61 17.1 | |

# Chapter 6

# Conclusion

In the present work, we studied two huge dust structures in the NGC3603 using 60$\mu$m and 100$\mu$m IRAS maps taken from IRAS satellite. Our motive is to study the physical properties of the clumps which are considered to be a star forming region. We have calculated dust color temperature profile and mass profile of the region of interest. In addition, flux density variation, discrete sources around the maxima and inclination angle of the clumps were studied. For the image processing, software ALADIN is used. We conclude our results as follows:

- Two clump centers are separated by 50.12 pc distance. The maximum and minimum dust color temperature of the large and small clump are 40.98 K, 27.39 K and 39.61 K, 24.80 K respectively. Thus, the coolest region lies on smaller clump.
- The mass of the gas in the larger and smaller clumps are found to be $1.20\times10^4 M_\odot$ and $1.50\times10^4 M_\odot$ respectively. Thus, smaller clump is found to be massive than that of the larger clump. Total mass of the both region is about $3.10\times10^4 M_\odot$. This mass exceeds the Jean's mass limit for the cloud of 90.41 pc diameter. Thus, Jean's criteria for the instability is fulfilled, suggesting active star forming region.
- Both the clumps seem to be isolated because of their Gussian like flux density distribution along the major and minor diameter.
- Both the clumps are neither face-on or edge-on type structure. Thus, true (3-dimensional) structure is sufficiently deep, indicating low temperature and high density.
- A large number of stars is found around 2 arcmin of the maxima of both the clumps, suggesting on going star formation.

## 6.1 Future Work

In the future, we intend to study the photometry of the stars in the region of interest as well as the value of initial mass function of both the clumps.

**REFERENCES**


Aryal B., Rajbahak C., Weinberger R., 2010, MNRAS, **402**, 2, 1307

Aryal B., Weinberger R., 2006, A&A, **448**, 213

Aryal B., Weinberger R., 2002, Dust Mass Estimation Using IRAS Maps, International Conference on 'Stellar Atmosphere', Sydney, Australia

Assendrop E., 1985, Ap&SS, **187**, 74

Balick B., Boeshaar G. O., Gull T. R., 1980, ApJ, **242**, 584

Basu S.K., 2007, Encyclopaedic Dictionary of Astrophysics, Global Vision Publishing House, India

Beichman C. A., Emerson J. P., Jennings R. E., Harris S., Baud B., Young E. T., 1985, Nearby Molecular Clouds, Proceedings of a Specialized Colloquium of the Eighth IAU European Regional Astronomy Meeting, Toulouse, France

Black J. H., Dalgarno A., 1976, ApJ, **203**, 132

Böhm-Vitense E., 1997, Introduction to Stellar Astrophysics, Cambridge University Press, UK

Brandl B., Brandner W., Eisenhauer F., Moffat A. F. J., Palla F., Zinnecker H., 1999, A&A, **352**, L69

Brandner W., Corcoran M. F., Brandl B., Ch, Y.-H., Grebel E. K., et al., 2000, HEAD, **5**, 4207

Clayton C. A., 1986, MNRAS, **219**, 895

Donofrio M., Rampazzo R., Bonfanti P., Longheffi M., Reduzzi L., et al., 1999, ApJ, **105**, 12

Drissen Laurent, Moffat Anthony F. J., Walborn Nolan R., Shara Michael M., 1995, AJ, **110**, 2235

Dupac X., Bernard J.P., Boudet N., Giard M., Lamarre J.M., et al., 2003, A&A, **404**, L11

Dyson J., 1997, Physics of the Interstellar Medium, London: Taylor & Francis

Eisenhauer F., Quirrenbach A., Zinnecker H., Genzel R., 1998, ApJ, **498**, 278

Enoch Melissa L., Young Kaisa E., Glenn Jason, Evans Neal J. II, Golwala Sunil, Sargent Anneila I., Harvey Paul, Aguirre James, Goldin Alexey, Hai Douglas, Huard Tracy L., Lange Andrew, Laurent Glenn, Maloney Philip, Mauskopf Philip, Rossinot Philippe, Sayers Jack, 2006, ApJ, **638**, 293

Frogel J. A., Persson S. E., Aaronson M., 1977, ApJ, **213**, 723

Glassgold A. E., Langer W. D., 1976, Bulletin of the American Astronomical Society, **8**, 322

Goss, W. M., Radhakrishnan V., 1969, Astrophysics Letter, **4**, 199

Herter T., 2012, Lecture on The Milky Way Galaxy, Cornell University [online], USA, Available from http://www.astro.cornell.edu/academics/courses/astro101/lectures/lec26.htm , [Accessed 19 January 2012]

Hildebrand R.H., 1983, QJRAS, **24**, 267

Hofmann K.-H., Seggewiss W., Weigelt G., 1995, A&A, **300**, 403

Holmberg E., Medd. Lund Astron. Obs. Ser., **VI** (117): 1

Johnstone D., Adams F. C., Lin D. N. C., Neufeeld D. A., Ostriker E. C., 2004, Star Formation in the Interstellar Medium: In Honor of David Hollenbach, Chris McKee, and Frank Shu, ASP Conference Series, **323**

Karttunen H., Kröger P., Oja H., Poutanen M., Donner K.J., 2007, Fundamental Astronomy, Springer Publication

Keene J., Blake G. A., Phillips T. G., Huggins P. J., Beichman C. A., 1985, ApJ, **299**, 967

Kundt Wolfgang, 2005, Astrophysics- A New Approach, **Second Edition**, Springer Publishers, Germany

Meaburn J., Redman M.P., O'Connor J.A., Holloway A.J., Bryce M., 2000, MNRAS, **312**, 23

Melnick J., Grosbol P., 1982, A&A, **107**, 23

Melnick G., Gull G. E., Harwit M., 1979, ApJ, **227**, L29

Melnick J., Tapia M., Terlevich R., 1989, A&A, **213**, 80

Moffat Anthony F. J., 1974, A & A, **35**, 315

Moffat Anthony F. J., 1983, A&A, **124**, 273

Moffat Anthony F. J., Niemela V. S., 1984, ApJ, **284**, 631

Moffat Anthony F. J., Drissen Laurent, Shara Michael M., 1994, ApJ, **436**, 183

Neugebauer G., Habing H. J., van Duinen R., Aumann H. H., Baud B., Beichman C. A., Beintema D. A., Boggess N., Clegg P. E., de Jong T., Emerson J. P., Gautier T. N., Gillett F. C., Harris S., Hauser M. G., Houck J. R., Jennings R. E., Low F. J., Marsden P. L., Miley G., Olnon F. M., Pottasch S. R., Raimond E., Rowan-Robinson M., Soifer B. T., Walker R. G., Wesselius P. R., Young E., 1984, ApJ, **273**, L1

Nürnberger D. E. A., 2003, A& A, **404**, 255

Nürnberger D. E. A., Petr-Gotzens M. G., 2002, A& A, **382**, 537

Nürnberger D. E. A., Stanke T., 2003, A&A , **400**, 223

Odenwald S.F., Rickard L.J., 1987, ApJ, **318**, 702

Palen S.E., 2000, Theory and Problems of Astronomy, McGraw-Hill, USA

Pandey Anil K., Ogura Katsuo, Sekiguchi Kaz, 2000, PASJ, **52**, 847

Phillips T. G., Huggins P. J., 1981, ApJ, **251**, 533

Schnee S.L., Ridge N.A., Goodman A.A., Jason G.L., 2005, ApJ **634**, 442

Simkhada K., 2006, A New Symmetrical Far Infrared Nebula at $-33°$ Declination, M.Sc. Thesis, Tribhuvan University, Kirtipur, Nepal

Smith H.E., 2012, Gene Smith's Astronomy Tutorial, University of California, San Diego [online] USA, Available from http://casswww.ucsd.edu/archive/public/tutorial/ISM.html [Accessed 21 January 2012]

Socker Noam, Hadar Ron, 2002, MNRAS, **331**, 731

Spitzer L. Jr., Jenkins E. B., 1975, Annual review of astronomy and astrophysics, **13**, 133

Storey J. W. V., Watson D. M., Townes C. H., 1979, ApJ, **233**, 109

Tielens A.G.G.M., 2005, The Physics and Chemistry of the Interstellar Medium, Cambridge University Press, UK

Van den Bergh S., 1978, A&A, **63**, 275

Van den Bos W. H., 1928, Bulletin of the Astronomical Institutes of the Netherlands, **4**, 261

Walborn Nolan R., 1973, ApJ, **182**, L21

Web[1]: http://www.astronet.ru/db/xware/msg/1163138

Web[2]: http://www.astro.ucla.edu/∼wright/WISE/ERO-NGC_3603.jpg

Web[3]: http://www.eso.org/gallery/v/ESOPIA/StarClusters/phot-38a-99.tif.html

Web[4]: http://aladin.u-strasbg.fr/java/alapre.pl?-c=NGC3603&button=RGB]

Web[5]: http://ej.iop.org/images/1538- 3881/119/1/292/Full/fg1.t.gif

Web[6]: http://aladin.u-strasbg.fr/

Young K., Phillips T.G., Knapp G.R.,1993, ApJ, **409**, 725

Note: The full form of abbreviation of the Astrophysical journals are given in the abbreviation chapter.

# Appendix A

# Database

Table A.1: Mass and temperature profile of small clump with positions of each pixels.

| R.A. Hr Min Sec | Dec. Deg Min Sec | Flux (60) | Flux (100) | R | Temperature (K) | Plank Function | Mass $M_\odot$ |
|---|---|---|---|---|---|---|---|
| 11 12 19.08 | -61 16 41.8 | 4892.491 | 8236.944 | 0.593969195 | 31.21894427 | 3.99341E-15 | 1.210859611 |
| 11 12 06.50 | -61 16 34.6 | 9300.191 | 10483.044 | 0.887165121 | 35.90325496 | 7.3479E-15 | 0.837521625 |
| 11 11 53.93 | -61 16 20.9 | 10889.391 | 12157.144 | 0.895719505 | 36.03257227 | 7.45637E-15 | 0.95714156 |
| 11 11 43.13 | -61 16 33.2 | 8245.991 | 8023.644 | 1.027711474 | 37.99281341 | 9.2022E-15 | 0.511860875 |
| 11 12 17.19 | -61 18 12.4 | 7556.591 | 10910.944 | 0.692569864 | 32.86012159 | 5.0404E-15 | 1.270776149 |
| 11 12 05.49 | -61 18 18.3 | 13598.591 | 17521.144 | 0.776124607 | 34.19326651 | 5.99307E-15 | 1.716266997 |
| 11 11 53.81 | -61 18 04.6 | 16171.991 | 18775.644 | 0.861328165 | 35.51073546 | 7.02382E-15 | 1.569255285 |
| 11 11 41.22 | -61 17 57.3 | 12859.391 | 15137.744 | 0.849491906 | 35.32990236 | 6.87713E-15 | 1.292189499 |
| 11 11 29.54 | -61 17 50.0 | 6938.691 | 8700.244 | 0.797528322 | 34.52782773 | 6.24646E-15 | 0.817654246 |
| 11 12 16.20 | -61 19 36.6 | 7610.091 | 11283.544 | 0.674441558 | 32.56446848 | 4.84152E-15 | 1.368155615 |
| 11 12 04.51 | -61 19 29.5 | 13063.591 | 17200.844 | 0.759473837 | 33.93116364 | 5.79857E-15 | 1.741410378 |
| 11 11 52.80 | -61 19 28.8 | 16898.791 | 21439.544 | 0.788206643 | 34.38243816 | 6.13564E-15 | 2.051292162 |
| 11 11 41.11 | -61 19 21.5 | 12305.891 | 17748.744 | 0.693338695 | 32.87260572 | 5.0489E-15 | 2.063682318 |
| 11 11 29.42 | -61 19 14.2 | 6282.191 | 9378.444 | 0.669854296 | 32.48925374 | 4.79165E-15 | 1.148994417 |
| 11 12 05.30 | -61 21 06.7 | 9215.091 | 13287.944 | 0.693492613 | 32.87510448 | 5.0506E-15 | 1.544495532 |
| 11 11 51.81 | -61 20 46.5 | 10263.991 | 15640.844 | 0.656229996 | 32.26487238 | 4.64459E-15 | 1.976899218 |
| 11 11 40.10 | -61 20 45.7 | 8164.791 | 14147.744 | 0.577109043 | 30.92930811 | 3.82307E-15 | 2.172436251 |
| 11 12 01.61 | -61 22 24.3 | 6219.591 | 7497.844 | 0.829517259 | 35.02320949 | 6.63212E-15 | 0.663676171 |
| 11 11 50.79 | -61 22 23.6 | 4733.191 | 9377.244 | 0.504752889 | 29.64963016 | 3.12203E-15 | 1.763237489 |
| 11 11 39.07 | -61 22 16.3 | 3857.991 | 8349.244 | 0.462076686 | 28.86217606 | 2.73213E-15 | 1.79398293 |
| 11 11 56.04 | -61 12 01.8 | 602.431 | 1097.144 | 0.549090183 | 30.44120048 | 3.54577E-15 | 0.181645903 |
| 11 12 44.37 | -61 14 01.0 | 383.161 | 1106.644 | 0.346236911 | 26.55777871 | 1.7683E-15 | 0.367387555 |
| 11 12 32.70 | -61 14 00.5 | 537.521 | 1285.544 | 0.418127268 | 28.02021798 | 2.34972E-15 | 0.321175621 |
| 11 12 21.05 | -61 13 40.5 | 1199.291 | 2103.244 | 0.570210114 | 30.80993064 | 3.75412E-15 | 0.328892446 |
| 11 12 09.39 | -61 13 33.4 | 1823.791 | 2172.944 | 0.839317994 | 35.17393468 | 6.75193E-15 | 0.188926329 |
| 11 11 57.73 | -61 13 32.7 | 2120.991 | 2156.944 | 0.98333151 | 37.34047026 | 8.6002E-15 | 0.147232081 |
| 11 11 43.37 | -61 13 31.7 | 1342.291 | 1798.144 | 0.746486933 | 33.72556535 | 5.64846E-15 | 0.186881693 |
| 11 11 30.82 | -61 13 17.9 | 778.191 | 1206.444 | 0.645028696 | 32.0792508 | 4.52491E-15 | 0.15651994 |
| 11 12 44.30 | -61 15 31.7 | 557.771 | 1629.844 | 0.34222355 | 26.47239445 | 1.73753E-15 | 0.55066397 |
| 11 12 31.73 | -61 15 24.7 | 1363.891 | 3052.344 | 0.446833974 | 28.57401133 | 2.59726E-15 | 0.689905665 |
| 11 12 19.17 | -61 15 11.1 | 2084.591 | 4209.444 | 0.495217658 | 29.47600851 | 3.03336E-15 | 0.814653755 |
| 11 12 06.61 | -61 14 57.4 | 4190.591 | 5541.944 | 0.75615903 | 33.87878547 | 5.76012E-15 | 0.564810459 |
| 11 11 54.93 | -61 14 56.7 | 4920.891 | 5145.644 | 0.956321697 | 36.94028202 | 8.24121E-15 | 0.366539377 |
| 11 11 42.37 | -61 14 49.4 | 3102.191 | 3225.644 | 0.961727643 | 37.02058197 | 8.31261E-15 | 0.227798545 |
| 11 11 30.69 | -61 14 48.6 | 2404.091 | 2493.044 | 0.964319523 | 37.05904509 | 8.34692E-15 | 0.175337769 |
| 11 11 19.01 | -61 14 54.2 | 652.901 | 1095.444 | 0.596014949 | 31.25388996 | 4.01426E-15 | 0.160197894 |
| 11 12 55.92 | -61 17 02.8 | 431.801 | 1347.144 | 0.320530693 | 26.0028334 | 1.57441E-15 | 0.502304281 |
| 11 12 45.13 | -61 17 02.4 | 701.201 | 2476.544 | 0.283136904 | 25.15754349 | 1.30637E-15 | 1.112888921 |
| 11 12 31.65 | -61 17 01.9 | 1865.491 | 4478.244 | 0.416567521 | 27.98968598 | 2.33652E-15 | 1.125151206 |
| 11 11 30.56 | -61 16 19.3 | 4321.891 | 3792.644 | 1.139545657 | 39.61215603 | 1.07853E-14 | 0.206435231 |
| 11 11 17.08 | -61 16 18.3 | 1597.591 | 1724.844 | 0.926223473 | 36.49124707 | 7.84783E-15 | 0.129024461 |
| 11 13 06.65 | -61 18 46.8 | 402.051 | 1140.744 | 0.352446298 | 26.68901774 | 1.81627E-15 | 0.368705908 |
| 11 12 54.96 | -61 18 40.0 | 453.321 | 1399.444 | 0.323929361 | 26.07733392 | 1.59961E-15 | 0.513587046 |
| 11 12 43.27 | -61 18 26.6 | 1163.291 | 2526.444 | 0.460445987 | 28.83153153 | 2.71759E-15 | 0.545755694 |
| 11 12 30.67 | -61 18 26.0 | 2303.291 | 6203.944 | 0.371262378 | 27.08059073 | 1.96428E-15 | 1.854117261 |
| 11 11 16.93 | -61 17 55.5 | 2454.091 | 2799.044 | 0.876760422 | 35.7455415 | 7.21675E-15 | 0.227687821 |
| 11 11 02.56 | -61 17 41.3 | 615.331 | 1317.044 | 0.467206107 | 28.95828982 | 2.77804E-15 | 0.278313485 |
| 11 13 06.61 | -61 20 04.6 | 382.791 | 1128.744 | 0.339130042 | 26.40627324 | 1.71393E-15 | 0.386610489 |
| 11 12 54.91 | -61 19 57.8 | 493.971 | 1406.644 | 0.351169877 | 26.66212439 | 1.80637E-15 | 0.457139757 |
| 11 12 43.20 | -61 19 57.3 | 1209.291 | 2427.644 | 0.498133581 | 29.52923823 | 3.06038E-15 | 0.465673765 |
| 11 12 30.60 | -61 19 50.3 | 3566.891 | 5525.844 | 0.645492526 | 32.08695815 | 4.52984E-15 | 0.716123293 |
| 11 11 15.91 | -61 19 13.2 | 1565.391 | 3687.144 | 0.424553801 | 28.14552099 | 2.4044E-15 | 0.900235094 |
| 11 11 02.40 | -61 19 18.5 | 628.491 | 1533.544 | 0.409829128 | 27.85722983 | 2.27976E-15 | 0.394892177 |
| 11 13 04.76 | -61 21 28.8 | 424.311 | 1084.744 | 0.391162339 | 27.48542121 | 2.12506E-15 | 0.299659533 |
| 11 12 53.94 | -61 21 28.4 | 538.551 | 1322.644 | 0.407177593 | 27.80485886 | 2.25756E-15 | 0.343934122 |
| 11 12 41.33 | -61 21 21.5 | 938.591 | 2010.944 | 0.466741491 | 28.94960129 | 2.77387E-15 | 0.42558492 |
| 11 12 29.63 | -61 21 08.0 | 2104.191 | 3986.944 | 0.527770393 | 30.06367796 | 3.33968E-15 | 0.700822296 |
| 11 12 17.91 | -61 21 13.9 | 5658.791 | 6780.644 | 0.834550671 | 35.1006776 | 6.69355E-15 | 0.594683866 |
| 11 11 26.58 | -61 20 44.7 | 2631.391 | 6341.744 | 0.41493176 | 27.95761477 | 2.3227E-15 | 1.602833496 |
| 11 11 15.78 | -61 20 37.4 | 1550.091 | 3704.144 | 0.418474822 | 28.02701488 | 2.35267E-15 | 0.92427105 |
| 11 11 02.27 | -61 20 36.3 | 574.801 | 1518.744 | 0.378471289 | 27.22830197 | 2.02202E-15 | 0.440931019 |
| 11 12 52.97 | -61 23 05.6 | 645.961 | 1272.344 | 0.507693674 | 29.7029231 | 3.14955E-15 | 0.237152747 |
| 11 12 41.26 | -61 22 45.7 | 949.591 | 1727.944 | 0.549549638 | 30.44927627 | 3.55025E-15 | 0.285721047 |
| 11 12 28.63 | -61 22 51.6 | 1604.591 | 2619.044 | 0.612662865 | 31.53674012 | 4.1853E-15 | 0.367357197 |
| 11 12 16.93 | -61 22 31.6 | 4056.691 | 4558.544 | 0.889909366 | 35.94477387 | 7.38264E-15 | 0.362482233 |
| 11 11 26.46 | -61 22 09.0 | 2277.691 | 5173.844 | 0.440231866 | 28.44796912 | 2.53958E-15 | 1.195978672 |
| 11 11 14.73 | -61 22 14.5 | 943.091 | 2201.044 | 0.428474397 | 28.22157833 | 2.43796E-15 | 0.529997095 |
| 11 11 01.23 | -61 22 00.4 | 471.681 | 1360.744 | 0.346634635 | 26.56621613 | 1.77136E-15 | 0.450964308 |
| 11 12 52.92 | -61 24 23.4 | 481.391 | 1158.344 | 0.415585526 | 27.97043901 | 2.32822E-15 | 0.292069544 |
| 11 12 41.19 | -61 24 16.4 | 888.991 | 1412.744 | 0.629265458 | 31.81620628 | 4.35834E-15 | 0.190289163 |
| 11 12 27.65 | -61 24 15.8 | 1255.491 | 1915.744 | 0.655354264 | 32.25039804 | 4.6352E-15 | 0.242628253 |
| 11 12 15.93 | -61 24 08.8 | 1660.591 | 2618.444 | 0.63419 | 31.89861764 | 4.41014E-15 | 0.348548068 |
| 11 12 03.30 | -61 24 01.6 | 2558.991 | 3271.144 | 0.782292372 | 34.28994114 | 6.0657E-15 | 0.316585107 |
| 11 11 50.66 | -61 24 00.8 | 2460.391 | 3710.044 | 0.663170302 | 32.37936118 | 4.7193E-15 | 0.461501721 |
| 11 11 38.94 | -61 23 53.5 | 1948.291 | 4387.444 | 0.444060597 | 28.52115693 | 2.57298E-15 | 1.001031338 |
| 11 11 26.31 | -61 23 52.6 | 1095.191 | 2650.644 | 0.413179212 | 27.92319516 | 2.30792E-15 | 0.674221854 |
| 11 11 12.79 | -61 23 38.6 | 618.891 | 1691.544 | 0.365873427 | 26.96935306 | 1.92148E-15 | 0.516795287 |
| 11 12 39.31 | -61 25 53.6 | 512.401 | 1221.144 | 0.419607352 | 28.04914678 | 2.36228E-15 | 0.303464822 |
| 11 12 26.66 | -61 25 53.0 | 740.571 | 1371.544 | 0.539954241 | 30.28010039 | 3.45693E-15 | 0.232911797 |
| 11 12 15.83 | -61 25 46.0 | 665.751 | 1667.044 | 0.399360185 | 27.64961295 | 2.19254E-15 | 0.446345423 |
| 11 12 02.29 | -61 25 38.7 | 681.351 | 1929.944 | 0.35304185 | 26.70155081 | 1.82089E-15 | 0.622203412 |
| 11 11 49.65 | -61 25 31.5 | 1157.791 | 1851.844 | 0.625209791 | 31.74817203 | 4.31584E-15 | 0.251889803 |
| 11 11 35.21 | -61 25 24.0 | 810.191 | 1720.344 | 0.47094709 | 29.02812349 | 2.81169E-15 | 0.359186874 |
| 11 11 23.47 | -61 25 23.1 | 603.221 | 1579.344 | 0.381944022 | 27.29902322 | 2.05004E-15 | 0.45225748 |
| 11 12 01.29 | -61 26 56.4 | 288.581 | 1076.844 | 0.267987749 | 24.80016409 | 1.20269E-15 | 0.525620428 |

Table A.2: Mass and temperature profile of large clump with positions of each pixels.

| R.A. Hr Min Sec | Dec. Deg Min Sec | Flux (60) | Flux (100) | R | Temperature (K) | Plank Function | Mass $M_\odot$ |
|---|---|---|---|---|---|---|---|
| 11 15 17.74 | -61 10 14.9 | 10963.991 | 9412.044 | 1.164889476 | 39.97498387 | 1.1157E-14 | 0.495232729 |
| 11 15 04.30 | -61 10 02.3 | 10256.091 | 9944.444 | 1.031338806 | 38.04586379 | 9.25207E-15 | 0.630977188 |
| 11 14 52.65 | -61 10 02.5 | 7519.391 | 8650.544 | 0.869239091 | 35.6312366 | 7.12249E-15 | 0.712990727 |
| 11 15 16.90 | -61 11 39.1 | 11574.791 | 10999.144 | 1.052335618 | 38.35219741 | 9.54269E-15 | 0.67664393 |
| 11 15 04.34 | -61 11 33.0 | 15249.991 | 13261.144 | 1.149975522 | 39.7616379 | 1.09377E-14 | 0.711752196 |
| 11 14 50.89 | -61 11 33.3 | 12140.491 | 11322.944 | 1.072202689 | 38.64091842 | 9.82074E-15 | 0.676842013 |
| 11 15 16.06 | -61 13 16.3 | 13675.491 | 11894.944 | 1.149689397 | 39.75754026 | 1.09335E-14 | 0.638670261 |
| 11 15 02.60 | -61 13 16.7 | 16860.891 | 14648.044 | 1.151067747 | 39.7772782 | 1.09537E-14 | 0.785041055 |
| 11 14 50.92 | -61 12 57.5 | 16213.291 | 13313.544 | 1.21780429 | 40.72838225 | 1.19484E-14 | 0.654118643 |
| 11 14 38.37 | -61 13 04.2 | 9506.891 | 8527.444 | 1.114858215 | 39.25736703 | 1.04277E-14 | 0.480065912 |
| 11 15 25.09 | -61 14 46.8 | 9682.491 | 8080.144 | 1.198306738 | 40.45139356 | 1.16544E-14 | 0.407007145 |
| 11 15 14.31 | -61 14 47.1 | 14231.391 | 12370.344 | 1.15044424 | 39.7683501 | 1.09445E-14 | 0.663524537 |
| 11 15 01.74 | -61 14 53.9 | 17239.091 | 15619.444 | 1.10369428 | 39.09646235 | 1.02676E-14 | 0.893039289 |
| 11 14 50.96 | -61 14 34.7 | 16583.791 | 14086.044 | 1.177320687 | 40.15246449 | 1.1341E-14 | 0.729134773 |
| 11 14 38.39 | -61 14 34.9 | 11527.791 | 9287.744 | 1.241183112 | 41.05962802 | 1.23046E-14 | 0.44311362 |
| 11 15 26.95 | -61 16 17.4 | 12437.091 | 11361.344 | 1.094684837 | 38.96639024 | 1.0139E-14 | 0.65782154 |
| 11 15 12.56 | -61 16 11.4 | 15160.591 | 14747.644 | 1.028000879 | 37.99704745 | 9.20618E-15 | 0.940405954 |
| 11 15 01.77 | -61 15 58.7 | 17814.491 | 16445.644 | 1.083234624 | 38.80078838 | 9.97642E-15 | 0.967716889 |
| 11 14 49.19 | -61 15 59.0 | 16259.691 | 13722.744 | 1.184871699 | 40.26012029 | 1.14534E-14 | 0.703360522 |
| 11 14 38.40 | -61 15 46.2 | 9745.991 | 8336.744 | 1.169040455 | 40.03428218 | 1.12183E-14 | 0.436255384 |
| 11 15 37.81 | -61 17 54.2 | 9071.391 | 8422.344 | 1.077062514 | 38.71138387 | 9.8892E-15 | 0.499969632 |
| 11 15 26.10 | -61 17 35.2 | 13553.091 | 12397.344 | 1.093225371 | 38.94530064 | 1.01182E-14 | 0.719279622 |
| 11 15 12.61 | -61 17 42.1 | 16513.291 | 17283.644 | 0.955428786 | 36.92700869 | 8.22944E-15 | 1.232925929 |
| 11 15 01.81 | -61 17 29.4 | 16087.691 | 16101.844 | 0.999121032 | 37.57327562 | 8.81265E-15 | 1.072607754 |
| 11 14 48.32 | -61 17 29.7 | 12792.391 | 11790.644 | 1.084961178 | 38.82578038 | 1.00009E-14 | 0.692105048 |
| 11 14 37.53 | -61 17 10.4 | 8628.091 | 7719.244 | 1.117737825 | 39.29882263 | 1.04692E-14 | 0.432845727 |
| 11 15 37.87 | -61 19 12.0 | 6500.591 | 8287.544 | 0.784380873 | 34.3226272 | 6.09037E-15 | 0.798829885 |
| 11 15 24.37 | -61 19 19.0 | 11419.291 | 12661.144 | 0.901916209 | 36.12605587 | 7.5353E-15 | 0.986380159 |
| 11 15 12.66 | -61 19 12.8 | 13412.291 | 15263.744 | 0.878702565 | 35.77501625 | 7.24117E-15 | 1.237440614 |
| 11 15 01.85 | -61 19 00.2 | 12158.791 | 14046.544 | 0.865607298 | 35.57595166 | 7.07713E-15 | 1.165157221 |
| 11 14 49.25 | -61 19 00.4 | 9170.391 | 9842.744 | 0.931690492 | 36.57306247 | 7.91876E-15 | 0.729677364 |
| 11 15 25.32 | -61 20 43.2 | 7133.891 | 9102.744 | 0.783707748 | 34.31209517 | 6.08241E-15 | 0.878553665 |
| 11 15 13.61 | -61 20 37.1 | 7378.091 | 10663.644 | 0.691892096 | 32.8491125 | 5.03292E-15 | 1.243821027 |
| 11 15 00.09 | -61 20 30.9 | 7946.491 | 9525.344 | 0.834247141 | 35.09600961 | 6.68984E-15 | 0.835866083 |
| 11 15 30.87 | -61 02 47.3 | 610.481 | 1082.844 | 0.563775576 | 30.69812191 | 3.6902E-15 | 0.172261368 |
| 11 16 20.08 | -61 04 41.5 | 727.001 | 1160.844 | 0.626269335 | 31.76596035 | 4.32693E-15 | 0.157494596 |
| 11 16 08.45 | -61 04 29.3 | 910.091 | 1362.844 | 0.667788096 | 32.45532115 | 4.76924E-15 | 0.167752413 |
| 11 15 55.05 | -61 04 23.5 | 1051.891 | 1564.844 | 0.67220183 | 32.52776559 | 4.81715E-15 | 0.190701009 |
| 11 15 44.33 | -61 04 23.9 | 1067.991 | 1594.844 | 0.66965233 | 32.48593841 | 4.78946E-15 | 0.195480766 |
| 11 15 30.93 | -61 04 18.0 | 1046.391 | 1566.844 | 0.667833556 | 32.45606809 | 4.76973E-15 | 0.192842849 |
| 11 15 19.32 | -61 04 11.9 | 808.351 | 1625.844 | 0.497188537 | 29.51199978 | 3.05161E-15 | 0.312767399 |
| 11 15 05.92 | -61 04 05.8 | 708.161 | 1437.844 | 0.492515878 | 29.42657989 | 3.0084E-15 | 0.280574928 |
| 11 14 53.42 | -61 04 12.6 | 596.021 | 1322.844 | 0.450560308 | 28.64481846 | 2.63001E-15 | 0.29527212 |
| 11 16 19.29 | -61 06 12.3 | 859.911 | 1255.844 | 0.684727562 | 32.73252825 | 4.95402E-15 | 0.148816089 |
| 11 16 06.76 | -61 06 00.1 | 1251.591 | 1629.844 | 0.767920734 | 34.06433405 | 5.89695E-15 | 0.162252122 |
| 11 15 54.25 | -61 06 00.7 | 1580.091 | 2018.844 | 0.782671172 | 34.29587139 | 6.07017E-15 | 0.195242155 |
| 11 15 42.62 | -61 05 54.7 | 1636.091 | 2059.844 | 0.794279081 | 34.47720424 | 6.20775E-15 | 0.19479246 |
| 11 15 30.10 | -61 05 42.3 | 1509.391 | 2322.844 | 0.649803 | 32.15849682 | 4.57579E-15 | 0.298006979 |
| 11 15 18.48 | -61 05 49.1 | 1543.291 | 2255.844 | 0.684130197 | 32.72279024 | 4.94746E-15 | 0.267669304 |
| 11 15 05.07 | -61 05 36.6 | 1292.991 | 2212.844 | 0.584311863 | 31.0534038 | 3.89552E-15 | 0.333470048 |
| 11 14 52.56 | -61 05 43.3 | 1099.991 | 1922.844 | 0.572064608 | 30.84207083 | 3.77261E-15 | 0.299208753 |
| 11 14 41.83 | -61 05 37.0 | 802.571 | 1602.844 | 0.500716851 | 29.57629531 | 3.08439E-15 | 0.30506644 |
| 11 14 28.43 | -61 05 30.7 | 675.851 | 1220.844 | 0.553593252 | 30.52024443 | 3.58984E-15 | 0.19964431 |
| 11 16 18.48 | -61 07 30.1 | 794.811 | 1270.844 | 0.6254198 | 31.75169861 | 4.31804E-15 | 0.172773608 |
| 11 16 07.75 | -61 07 37.2 | 1328.591 | 1729.844 | 0.768040933 | 34.06622598 | 5.89836E-15 | 0.172166193 |
| 11 15 54.32 | -61 07 24.9 | 1846.291 | 2327.844 | 0.793133475 | 34.45934169 | 6.19412E-15 | 0.220620596 |
| 11 15 41.80 | -61 07 25.5 | 2414.491 | 2912.844 | 0.828911881 | 35.01388373 | 6.62474E-15 | 0.258119187 |
| 11 15 30.17 | -61 07 26.0 | 2272.291 | 3271.844 | 0.694498576 | 32.89143141 | 5.06173E-15 | 0.379459764 |
| 11 15 16.74 | -61 07 13.4 | 2437.091 | 3827.844 | 0.636674588 | 31.94011522 | 4.43636E-15 | 0.506523525 |
| 11 15 05.11 | -61 07 00.8 | 2776.891 | 4021.844 | 0.690452191 | 32.82571257 | 5.01703E-15 | 0.470598949 |
| 11 14 53.48 | -61 07 07.5 | 2317.191 | 3305.844 | 0.700937794 | 32.99576541 | 5.13316E-15 | 0.378067936 |
| 11 14 40.96 | -61 07 01.3 | 1461.891 | 2691.844 | 0.54308162 | 30.33535952 | 3.48725E-15 | 0.453146691 |
| 11 14 27.55 | -61 07 07.9 | 1120.291 | 1898.844 | 0.589985802 | 31.15077863 | 3.95293E-15 | 0.281995178 |
| 11 14 15.92 | -61 06 55.0 | 822.071 | 1438.844 | 0.571341299 | 30.82953962 | 3.76539E-15 | 0.224323857 |
| 11 14 04.29 | -61 06 55.0 | 641.471 | 1124.844 | 0.570275523 | 30.81106488 | 3.75477E-15 | 0.175865703 |
| 11 16 19.48 | -61 09 00.8 | 936.591 | 1245.844 | 0.751772293 | 33.80936542 | 5.70938E-15 | 0.128099343 |
| 11 16 06.06 | -61 09 08.0 | 1245.591 | 1742.844 | 0.71468875 | 33.21757626 | 5.28687E-15 | 0.193522539 |
| 11 15 52.61 | -61 08 55.7 | 2343.191 | 2711.844 | 0.864058183 | 35.55235203 | 7.05781E-15 | 0.225562385 |
| 11 15 40.97 | -61 08 49.8 | 2771.891 | 3805.844 | 0.728324913 | 33.43624103 | 5.44089E-15 | 0.410632172 |
| 11 15 28.44 | -61 08 50.3 | 3582.591 | 5412.844 | 0.661868511 | 32.35791647 | 4.70526E-15 | 0.67532714 |
| 11 15 15.90 | -61 08 37.7 | 3764.991 | 6305.844 | 0.597063771 | 31.27178977 | 4.02496E-15 | 0.919715706 |
| 11 15 04.26 | -61 08 38.0 | 5215.691 | 7340.844 | 0.710502907 | 33.15019738 | 5.23991E-15 | 0.822420689 |
| 11 14 52.62 | -61 08 31.8 | 4153.591 | 5799.844 | 0.716155641 | 33.24115977 | 5.30337E-15 | 0.642002403 |
| 11 14 39.20 | -61 08 32.0 | 2697.091 | 3666.844 | 0.7355347 | 33.55135094 | 5.52296E-15 | 0.389755984 |
| 11 14 26.66 | -61 08 38.6 | 1740.891 | 2854.844 | 0.609802497 | 31.48833277 | 4.15573E-15 | 0.403280131 |
| 11 14 15.92 | -61 08 32.2 | 1198.691 | 1945.844 | 0.616026259 | 31.5935614 | 4.22015E-15 | 0.270677226 |
| 11 14 02.50 | -61 08 25.7 | 866.641 | 1372.844 | 0.631274202 | 31.84984836 | 4.37945E-15 | 0.184023795 |
| 11 16 29.46 | -61 10 50.3 | 809.631 | 1110.844 | 0.728843114 | 33.44452597 | 5.44677E-15 | 0.119725225 |
| 11 16 18.69 | -61 10 38.0 | 1016.091 | 1308.844 | 0.776327049 | 34.19644311 | 5.99545E-15 | 0.128155698 |
| 11 16 05.24 | -61 10 25.8 | 1539.191 | 1960.844 | 0.784963516 | 34.33174141 | 6.09726E-15 | 0.188790728 |
| 11 15 52.70 | -61 10 32.9 | 2423.891 | 3049.844 | 0.794759011 | 34.48468525 | 6.21346E-15 | 0.288148273 |
| 11 15 41.05 | -61 10 27.0 | 4367.891 | 4640.844 | 0.941184621 | 36.7148742 | 8.04249E-15 | 0.338749206 |
| 11 15 29.40 | -61 10 27.4 | 4987.791 | 6696.844 | 0.744797251 | 33.69873807 | 5.62903E-15 | 0.698407259 |
| 11 14 38.32 | -61 10 02.7 | 4088.191 | 5417.844 | 0.754578943 | 33.85379434 | 5.74182E-15 | 0.553922084 |
| 11 14 26.68 | -61 10 02.9 | 2883.591 | 3047.844 | 0.946108462 | 36.78828772 | 8.10694E-15 | 0.220702822 |

contd..

| R.A. Hr Min Sec | Dec. Deg Min Sec | Flux (60) | Flux (100) | R | Temperature (K) | Plank Function | Mass $M_{\odot}$ |
|---|---|---|---|---|---|---|---|
| 11 14 15.03 | -61 10 02.9 | 1714.791 | 2023.844 | 0.84729406 | 35.29625119 | 6.85001E-15 | 0.173443422 |
| 11 14 02.49 | -61 09 49.9 | 865.971 | 1322.844 | 0.65462821 | 32.2383928 | 4.62741E-15 | 0.167819579 |
| 11 16 40.34 | -61 12 26.8 | 851.251 | 1132.844 | 0.751428264 | 33.80391612 | 5.70541E-15 | 0.116561636 |
| 11 16 28.68 | -61 12 27.6 | 901.191 | 1188.844 | 0.758039743 | 33.90851137 | 5.78192E-15 | 0.120704844 |
| 11 16 17.90 | -61 12 08.8 | 1374.591 | 1604.844 | 0.856526242 | 35.43745117 | 6.96417E-15 | 0.135280573 |
| 11 16 06.23 | -61 11 56.5 | 1715.291 | 2293.844 | 0.747780145 | 33.74608562 | 5.66334E-15 | 0.237773377 |
| 11 15 52.79 | -61 12 10.1 | 3477.591 | 3255.844 | 1.068107379 | 38.58148977 | 9.76318E-15 | 0.195769223 |
| 11 15 42.01 | -61 11 51.2 | 5516.391 | 4974.844 | 1.108857082 | 39.17091031 | 1.03415E-14 | 0.282401697 |
| 11 15 29.46 | -61 11 51.7 | 8574.591 | 7285.844 | 1.176883694 | 40.14623079 | 1.13346E-14 | 0.377352503 |
| 11 14 36.55 | -61 11 33.5 | 7588.691 | 6876.844 | 1.103513618 | 39.09385602 | 1.0265E-14 | 0.393281485 |
| 11 14 24.90 | -61 11 46.6 | 3877.591 | 3699.844 | 1.048041755 | 38.28965395 | 9.48298E-15 | 0.229039499 |
| 11 14 13.24 | -61 11 40.1 | 1956.691 | 2000.844 | 0.977932812 | 37.26068121 | 8.52799E-15 | 0.137733102 |
| 11 14 01.59 | -61 11 20.7 | 835.541 | 1099.844 | 0.759690465 | 33.93458429 | 5.80108E-15 | 0.111299721 |
| 11 14 00.68 | -61 12 44.9 | 663.711 | 1095.844 | 0.605661937 | 31.41812145 | 4.11307E-15 | 0.156406588 |
| 11 14 12.35 | -61 13 04.4 | 2037.591 | 2041.844 | 0.997917079 | 37.5555527 | 8.79639E-15 | 0.136266867 |
| 11 14 24.91 | -61 13 10.8 | 5083.091 | 4212.844 | 1.206569956 | 40.56886796 | 1.17786E-14 | 0.2099676 |
| 11 14 12.35 | -61 14 28.6 | 1990.591 | 2340.844 | 0.850373199 | 35.34338935 | 6.88801E-15 | 0.199503609 |
| 11 14 24.02 | -61 14 41.5 | 4944.991 | 4330.844 | 1.141807694 | 39.64459585 | 1.08182E-14 | 0.235010949 |
| 11 13 58.87 | -61 15 52.8 | 818.381 | 1330.844 | 0.614933831 | 31.57511757 | 4.20882E-15 | 0.185625941 |
| 11 14 10.55 | -61 15 52.8 | 1978.791 | 2143.844 | 0.923010723 | 36.44311347 | 7.80626E-15 | 0.16122121 |
| 11 14 24.93 | -61 15 59.3 | 5007.691 | 4633.844 | 1.080677511 | 38.76375991 | 9.94025E-15 | 0.273663024 |
| 11 13 57.96 | -61 17 23.5 | 1025.191 | 1385.844 | 0.739759309 | 33.61864211 | 5.57125E-15 | 0.146027273 |
| 11 14 10.55 | -61 17 17.1 | 1941.691 | 2299.844 | 0.844270742 | 35.24992344 | 6.81277E-15 | 0.198173889 |
| 11 14 24.94 | -61 17 23.5 | 3437.191 | 4051.844 | 0.848302896 | 35.31170032 | 6.86245E-15 | 0.346613466 |
| 11 16 53.03 | -61 13 56.6 | 834.291 | 1098.844 | 0.75924426 | 33.92753819 | 5.7959E-15 | 0.111297938 |
| 11 16 41.36 | -61 13 57.5 | 882.871 | 1170.844 | 0.754046654 | 33.84537201 | 5.73566E-15 | 0.119835992 |
| 11 16 29.70 | -61 14 04.7 | 966.391 | 1235.844 | 0.781968436 | 34.28486915 | 6.06188E-15 | 0.119681833 |
| 11 16 17.11 | -61 13 46.1 | 1421.091 | 1608.844 | 0.883299437 | 35.84471432 | 7.29908E-15 | 0.129395155 |
| 11 16 04.54 | -61 13 40.3 | 2289.291 | 2408.844 | 0.95036914 | 36.85174158 | 8.16286E-15 | 0.173236175 |
| 11 15 52.86 | -61 13 34.4 | 3448.791 | 3627.844 | 0.950644791 | 36.85584454 | 8.16648E-15 | 0.260786933 |
| 11 15 40.29 | -61 13 22.0 | 5737.791 | 4643.844 | 1.235569283 | 40.98017235 | 1.22187E-14 | 0.223113033 |
| 11 15 28.62 | -61 13 15.9 | 8810.391 | 7349.844 | 1.198718095 | 40.45724463 | 1.16606E-14 | 0.370024977 |
| 11 16 54.04 | -61 15 14.3 | 810.831 | 1134.844 | 0.714486749 | 33.21432747 | 5.2846E-15 | 0.126065338 |
| 11 16 39.67 | -61 15 21.8 | 811.091 | 1153.844 | 0.702946846 | 33.02825638 | 5.15551E-15 | 0.131385387 |
| 11 16 28.90 | -61 15 22.5 | 824.671 | 1229.844 | 0.670549273 | 32.50065954 | 4.79919E-15 | 0.150436732 |
| 11 16 16.31 | -61 15 16.8 | 1312.691 | 1568.844 | 0.836725003 | 35.13410334 | 6.72016E-15 | 0.137047886 |
| 11 16 03.72 | -61 15 04.6 | 1933.091 | 2399.844 | 0.805506941 | 34.65189099 | 6.34187E-15 | 0.222145612 |
| 11 15 51.15 | -61 15 05.2 | 3551.091 | 3402.844 | 1.043565617 | 38.2244003 | 9.4209E-15 | 0.212041991 |
| 11 15 40.36 | -61 14 46.2 | 6569.091 | 5776.844 | 1.137141837 | 39.57767055 | 1.07502E-14 | 0.315460113 |
| 11 16 52.37 | -61 16 45.2 | 677.281 | 1073.844 | 0.630707067 | 31.84035375 | 4.37348E-15 | 0.144140358 |
| 11 16 39.79 | -61 16 52.6 | 688.751 | 1101.844 | 0.625089396 | 31.74615011 | 4.31459E-15 | 0.149917746 |
| 11 16 28.08 | -61 16 33.9 | 787.761 | 1191.844 | 0.660959824 | 32.34293929 | 4.69546E-15 | 0.149009219 |
| 11 16 15.51 | -61 16 41.1 | 1083.391 | 1589.844 | 0.681444846 | 32.67898121 | 4.91802E-15 | 0.189773839 |
| 11 16 03.82 | -61 16 41.8 | 2053.991 | 2432.844 | 0.844275671 | 35.249999 | 6.81283E-15 | 0.209632421 |
| 11 15 50.33 | -61 16 35.9 | 3661.791 | 4056.844 | 0.902620609 | 36.13667235 | 7.54429E-15 | 0.315676147 |
| 11 15 39.52 | -61 16 10.5 | 7270.891 | 6153.844 | 1.181520201 | 40.21235131 | 1.14035E-14 | 0.31679675 |
| 11 16 39.01 | -61 18 16.8 | 645.321 | 1108.844 | 0.581976365 | 31.01322572 | 3.87198E-15 | 0.168116151 |
| 11 16 27.29 | -61 18 04.7 | 774.971 | 1281.844 | 0.604575128 | 31.39966504 | 4.10189E-15 | 0.18345218 |
| 11 16 15.60 | -61 18 05.4 | 1532.791 | 1754.844 | 0.873462826 | 35.6954576 | 7.17537E-15 | 0.143570866 |
| 11 16 04.81 | -61 18 12.4 | 1883.491 | 2443.844 | 0.770708359 | 34.10818898 | 5.92955E-15 | 0.241948881 |
| 11 15 49.51 | -61 18 06.7 | 4465.891 | 4597.844 | 0.971301114 | 37.16253414 | 8.43961E-15 | 0.319818787 |
| 11 16 40.02 | -61 19 47.5 | 594.371 | 1215.844 | 0.488854656 | 29.35943062 | 2.97468E-15 | 0.239943681 |
| 11 16 28.31 | -61 19 41.8 | 950.091 | 1520.844 | 0.624712988 | 31.73982787 | 4.31065E-15 | 0.207116175 |
| 11 16 15.71 | -61 19 42.6 | 1261.191 | 1825.844 | 0.690744116 | 32.8304579 | 5.02025E-15 | 0.213506311 |
| 11 16 03.99 | -61 19 30.2 | 2857.891 | 2748.844 | 1.03967013 | 38.16756505 | 9.36698E-15 | 0.172275029 |
| 11 15 50.48 | -61 19 30.9 | 4337.291 | 4087.844 | 1.061021653 | 38.47856012 | 9.66389E-15 | 0.248321599 |
| 11 14 34.85 | -61 19 00.6 | 4606.091 | 5590.844 | 0.823863266 | 34.9360384 | 6.56335E-15 | 0.500062053 |
| 11 14 23.15 | -61 18 54.2 | 2989.691 | 3611.844 | 0.827746436 | 34.99592501 | 6.61055E-15 | 0.32074753 |
| 11 14 10.55 | -61 19 07.2 | 1731.591 | 2076.844 | 0.833760745 | 35.08852837 | 6.6839E-15 | 0.182408889 |
| 11 13 57.05 | -61 18 47.8 | 1044.891 | 1536.844 | 0.679893991 | 32.65365534 | 4.90104E-15 | 0.184082845 |
| 11 13 45.35 | -61 18 54.1 | 744.761 | 1182.844 | 0.629635861 | 31.82241243 | 4.36223E-15 | 0.15918082 |
| 11 16 39.24 | -61 21 11.8 | 608.401 | 1118.844 | 0.543776434 | 30.34762058 | 3.494E-15 | 0.187983069 |
| 11 16 27.52 | -61 21 12.6 | 829.711 | 1516.844 | 0.546998241 | 30.40439931 | 3.52535E-15 | 0.2525865 |
| 11 16 14.90 | -61 21 06.8 | 1419.191 | 1988.844 | 0.713575826 | 33.1996736 | 5.27437E-15 | 0.221361382 |
| 11 16 02.27 | -61 20 54.6 | 1990.791 | 2368.844 | 0.840406122 | 35.19063978 | 6.76528E-15 | 0.205552404 |
| 11 15 49.65 | -61 20 48.7 | 3606.591 | 3498.844 | 1.030795028 | 38.03791342 | 9.24459E-15 | 0.222182109 |
| 11 15 37.03 | -61 20 42.7 | 4897.391 | 5848.844 | 0.837326316 | 35.14334315 | 6.72752E-15 | 0.510372177 |
| 11 14 46.58 | -61 20 37.7 | 6026.391 | 7024.844 | 0.857868303 | 35.45794373 | 6.98082E-15 | 0.590747776 |
| 11 14 35.77 | -61 20 24.9 | 4085.391 | 4757.844 | 0.858664345 | 35.47009491 | 6.99071E-15 | 0.399540807 |
| 11 14 23.16 | -61 20 18.5 | 2333.891 | 2942.844 | 0.793073299 | 34.45840322 | 6.19341E-15 | 0.278939224 |
| 11 14 10.55 | -61 20 18.5 | 1597.791 | 2051.844 | 0.778709785 | 34.23381375 | 6.02348E-15 | 0.199971923 |
| 11 13 57.94 | -61 20 18.5 | 1056.491 | 1507.844 | 0.700663331 | 32.99132447 | 5.1301E-15 | 0.172544919 |
| 11 13 44.43 | -61 20 31.3 | 830.241 | 1280.844 | 0.648198375 | 32.1318841 | 4.55866E-15 | 0.164941837 |
| 11 13 32.72 | -61 20 18.2 | 600.441 | 1138.844 | 0.527237269 | 30.05416582 | 3.33458E-15 | 0.200491297 |
| 11 16 26.74 | -61 22 49.8 | 808.261 | 1461.844 | 0.552905098 | 30.50818025 | 3.58309E-15 | 0.239505178 |
| 11 16 15.01 | -61 22 50.5 | 1104.991 | 1760.844 | 0.627534864 | 31.78719355 | 4.34019E-15 | 0.23816836 |
| 11 16 00.56 | -61 22 31.8 | 1593.491 | 2214.844 | 0.7194597 | 33.29422552 | 5.34058E-15 | 0.243459407 |
| 11 15 48.84 | -61 22 25.9 | 2264.791 | 2632.844 | 0.860207061 | 35.49363535 | 7.00988E-15 | 0.220488946 |
| 11 15 37.11 | -61 22 26.4 | 3376.091 | 3714.844 | 0.908810976 | 36.22988396 | 7.62348E-15 | 0.286061421 |
| 11 15 23.58 | -61 22 14.0 | 4654.591 | 5706.844 | 0.815615601 | 34.80858611 | 6.4635E-15 | 0.518322908 |
| 11 15 10.96 | -61 22 14.3 | 5628.791 | 6529.844 | 0.862010027 | 35.52113301 | 7.0323E-15 | 0.545101349 |
| 11 15 00.14 | -61 22 21.1 | 4857.891 | 6072.844 | 0.799936735 | 34.56531367 | 6.2752E-15 | 0.568115114 |
| 11 14 46.61 | -61 22 14.9 | 3970.891 | 4800.844 | 0.827123522 | 34.98632351 | 6.60297E-15 | 0.426825354 |
| 11 14 33.99 | -61 21 49.1 | 3262.091 | 3790.844 | 0.860518396 | 35.4983847 | 7.01375E-15 | 0.317291075 |
| 11 14 21.37 | -61 21 55.7 | 2089.291 | 2564.844 | 0.814587944 | 34.79268089 | 6.4511E-15 | 0.233399287 |
| 11 14 10.55 | -61 22 02.2 | 1362.991 | 1930.844 | 0.705904257 | 33.07603187 | 5.18849E-15 | 0.218463178 |

contd..

| R.A. Hr Min Sec | Dec. Deg Min Sec | Flux (60) | Flux (100) | R | Temperature (K) | Plank Function | Mass $M_{\odot}$ |
|---|---|---|---|---|---|---|---|
| 11 13 57.93 | -61 21 49.2 | 888.791 | 1487.844 | 0.597368407 | 31.27698681 | 4.02807E-15 | 0.216836464 |
| 11 13 43.51 | -61 21 49.1 | 752.431 | 1271.844 | 0.591606361 | 31.17852976 | 3.96939E-15 | 0.188097317 |
| 11 13 32.69 | -61 21 42.4 | 561.391 | 1124.844 | 0.499083428 | 29.54655161 | 3.0692E-15 | 0.215148961 |
| 11 16 25.93 | -61 24 07.6 | 752.351 | 1294.844 | 0.581036017 | 30.99703261 | 3.86251E-15 | 0.196797461 |
| 11 16 13.29 | -61 24 08.4 | 917.291 | 1644.844 | 0.557676594 | 30.59171856 | 3.62997E-15 | 0.266007232 |
| 11 16 00.65 | -61 24 02.6 | 1185.591 | 1843.844 | 0.642999625 | 32.04551256 | 4.50334E-15 | 0.240359463 |
| 11 15 49.82 | -61 23 56.6 | 1530.491 | 2165.844 | 0.706648771 | 33.08804928 | 5.1968E-15 | 0.244659996 |
| 11 15 37.18 | -61 23 50.7 | 2051.791 | 2652.844 | 0.773430703 | 34.15097259 | 5.96145E-15 | 0.261235304 |
| 11 15 23.64 | -61 23 44.7 | 3168.191 | 2994.844 | 1.057881813 | 38.43290626 | 9.62001E-15 | 0.182755604 |
| 11 15 11.91 | -61 23 45.0 | 3421.391 | 3801.844 | 0.89992935 | 36.09609949 | 7.50996E-15 | 0.297186215 |
| 11 14 58.37 | -61 23 32.4 | 3555.391 | 3995.844 | 0.889772223 | 35.94269974 | 7.3809E-15 | 0.31781274 |
| 11 14 47.54 | -61 23 26.1 | 2987.491 | 3504.844 | 0.852389151 | 35.37422693 | 6.91293E-15 | 0.297631301 |
| 11 14 34.01 | -61 23 39.3 | 2722.991 | 2891.844 | 0.941610612 | 36.72122921 | 8.04806E-15 | 0.210938379 |
| 11 14 21.38 | -61 23 26.4 | 1965.191 | 2323.844 | 0.845663909 | 35.27127705 | 6.82992E-15 | 0.199739129 |
| 11 14 09.65 | -61 23 20.0 | 1028.791 | 1582.844 | 0.64996361 | 32.16115934 | 4.5775E-15 | 0.202993323 |
| 11 13 57.02 | -61 23 26.4 | 762.621 | 1375.844 | 0.554293219 | 30.53251012 | 3.59671E-15 | 0.224561782 |
| 11 13 45.29 | -61 23 19.8 | 594.751 | 1177.844 | 0.504948873 | 29.65318546 | 3.12386E-15 | 0.221344453 |
| 11 16 26.04 | -61 25 38.3 | 677.131 | 1264.844 | 0.535347442 | 30.19848485 | 3.41243E-15 | 0.217593245 |
| 11 16 13.38 | -61 25 26.1 | 781.301 | 1452.844 | 0.537773498 | 30.24149789 | 3.43584E-15 | 0.248232325 |
| 11 16 01.64 | -61 25 26.8 | 885.291 | 1679.844 | 0.527007865 | 30.05007163 | 3.33238E-15 | 0.295927928 |
| 11 15 48.09 | -61 25 27.4 | 985.591 | 1874.844 | 0.525692271 | 30.02657922 | 3.31982E-15 | 0.331530156 |
| 11 15 35.44 | -61 25 15.0 | 1231.791 | 1937.844 | 0.635650238 | 31.92301312 | 4.42554E-15 | 0.257053911 |
| 11 15 23.69 | -61 25 08.9 | 1332.091 | 2150.844 | 0.619334085 | 31.64934056 | 4.25453E-15 | 0.296776076 |
| 11 15 10.15 | -61 25 22.3 | 1901.791 | 2263.844 | 0.840071577 | 35.18550441 | 6.76118E-15 | 0.19656049 |
| 11 14 59.31 | -61 25 03.1 | 1966.691 | 2577.844 | 0.762920875 | 33.9855602 | 5.83865E-15 | 0.259189006 |
| 11 14 45.77 | -61 25 09.8 | 1994.191 | 2645.844 | 0.753706946 | 33.83999596 | 5.73174E-15 | 0.270988014 |
| 11 14 34.93 | -61 24 57.0 | 2010.191 | 2386.844 | 0.842196222 | 35.2181091 | 6.78727E-15 | 0.206443501 |
| 11 14 22.29 | -61 24 57.1 | 1305.791 | 1733.844 | 0.753119081 | 33.830691 | 5.72494E-15 | 0.177791579 |
| 11 14 08.74 | -61 24 50.7 | 945.091 | 1434.844 | 0.658671605 | 32.30519459 | 4.67083E-15 | 0.180336172 |
| 11 13 56.10 | -61 24 44.1 | 550.151 | 1144.844 | 0.480546695 | 29.20632723 | 2.89867E-15 | 0.231856765 |
| 11 13 45.27 | -61 24 37.6 | 482.931 | 1090.844 | 0.442713165 | 28.49542956 | 2.56121E-15 | 0.250028795 |
| 11 16 24.34 | -61 27 09.2 | 781.061 | 1273.844 | 0.613152788 | 31.54502353 | 4.19037E-15 | 0.178458035 |
| 11 16 10.77 | -61 26 57.0 | 802.931 | 1462.844 | 0.548883545 | 30.4375676 | 3.54375E-15 | 0.242330027 |
| 11 16 37.11 | -61 28 39.1 | 786.131 | 1238.844 | 0.634568194 | 31.90493776 | 4.41413E-15 | 0.164756883 |
| 11 16 00.82 | -61 26 57.5 | 736.281 | 1540.844 | 0.477842663 | 29.15627324 | 2.87407E-15 | 0.314725995 |
| 11 15 48.17 | -61 26 58.1 | 684.311 | 1502.844 | 0.455344001 | 28.73537227 | 2.67227E-15 | 0.330145925 |
| 11 15 35.50 | -61 26 39.2 | 616.401 | 1484.844 | 0.415128458 | 27.96147408 | 2.32436E-15 | 0.375016323 |
| 11 15 21.95 | -61 26 46.2 | 867.881 | 1517.844 | 0.571785375 | 30.83723383 | 3.76982E-15 | 0.23636233 |
| 11 15 07.48 | -61 26 33.6 | 872.331 | 1614.844 | 0.540195214 | 30.28436244 | 3.45926E-15 | 0.27404337 |
| 11 14 56.64 | -61 26 33.9 | 1283.191 | 1698.844 | 0.755331861 | 33.86570463 | 5.75054E-15 | 0.173427115 |
| 11 14 45.79 | -61 26 40.6 | 1366.091 | 1622.844 | 0.841788243 | 35.21184998 | 6.78225E-15 | 0.14046716 |
| 11 14 34.04 | -61 26 27.8 | 1211.591 | 1580.844 | 0.766420343 | 34.04071079 | 5.87943E-15 | 0.157843071 |
| 11 14 22.29 | -61 26 21.4 | 871.691 | 1420.844 | 0.613502256 | 31.55093081 | 4.19399E-15 | 0.198880124 |
| 11 14 09.64 | -61 26 14.9 | 614.811 | 1123.844 | 0.547060802 | 30.40550062 | 3.52596E-15 | 0.187111349 |
| 11 16 24.44 | -61 28 33.4 | 929.691 | 1386.844 | 0.670364511 | 32.49762765 | 4.79719E-15 | 0.169712197 |
| 11 16 12.67 | -61 28 27.6 | 833.281 | 1478.844 | 0.563467817 | 30.69276271 | 3.68715E-15 | 0.235452421 |
| 11 16 00.92 | -61 28 34.7 | 647.541 | 1425.844 | 0.454145755 | 28.7127259 | 2.66166E-15 | 0.314478583 |
| 11 15 47.34 | -61 28 28.9 | 463.331 | 1197.844 | 0.386804125 | 27.39753417 | 2.08948E-15 | 0.336538146 |
| 11 15 11.15 | -61 28 10.7 | 638.531 | 1181.844 | 0.540283658 | 30.28592657 | 3.46012E-15 | 0.20051246 |
| 11 14 57.58 | -61 28 04.6 | 731.551 | 1121.844 | 0.652096905 | 32.19650363 | 4.6003E-15 | 0.143158819 |
| 11 14 44.92 | -61 28 04.8 | 774.701 | 1196.844 | 0.64728653 | 32.11675144 | 4.54894E-15 | 0.154453993 |
| 11 16 35.40 | -61 29 57.0 | 848.071 | 1239.844 | 0.684014279 | 32.72090028 | 4.94619E-15 | 0.147152704 |
| 11 16 23.63 | -61 29 57.7 | 814.261 | 1344.844 | 0.605468738 | 31.41484135 | 4.11108E-15 | 0.1920384 |
| 11 16 12.78 | -61 30 11.3 | 660.441 | 1308.844 | 0.504598715 | 29.64683295 | 3.12058E-15 | 0.246220344 |
| 11 16 00.99 | -61 29 52.5 | 424.201 | 1076.844 | 0.393929854 | 27.54101321 | 2.14776E-15 | 0.294332981 |